Cyclic Delay Estimation Schemes in Time Domain Cyclic Selective Mapping for Orthogonal Frequency Division Multiplexing Systems

February 2017

A thesis submitted in partial fulfilment of the requirements for the degree of Doctor of Philosophy in Engineering

Keio University

Graduate School of Science and Technology
School of Integrated Design Engineering

Panca dewi pamungkasari

Contents

List of Figures

List of Tables

Acronyms

1G first generation

1xEV-DO 1x Evolution Data Only

1xEV-DOrA 1x Evolution Data Only revision A

2G second generation

3G third generation

3GPP third generation partnership project

ADSL asymetric digital subcriber

AWGN additive white Gaussian noise

BER bit error rate

CCDF complementary cumulative distribution function

CCDS combining of cyclically delayed signals

CCK complementary code keying

CDMA code division multiple access

CFO carrier frequency offset

CMs conversion matrices

CR clipping ratio combining of cyclically delayed signals (CCDS)

DAB digital audio broadcast

DC delayed correlation

DC-MF rdelayed correlation and matched filter

DFT discrete Fourier transform

DL ddownlink

DSSS direct sequence spread spectrum

FDE frequency domain equalization

FDM frequency division multiplexing

FDMA frequency division multiplexing access

FD-SLM frequency domain SLM

GI guard interval

GSM global system for mobile communications

HPA high power amplifier

HSDPA high speed downlink packet access

HSPA high speed packet access

IBO input back-off

ICI inter-carrier interference

IDFT inverse discrete Fourier transform

IEEE institute of electrical and electronics engineers

IFFT inverse fast Fourier transform

IMT international mobile telecommunication

IMT-A IMT-advanced

IQRC in-phase and quadrature recombination

ISI intersymbol interference

ITU international telecommunication union

JROF joint rotation and offset

LAN local area network

LC-SLM low complexity SLM

LOS line-of-sight

LTE long term evolution

LTE-A long term evolution-advanced

LTE (Rel.8) long term evolution (release 8)

MAC media access control

MCM multi-carrier modulation

MF matched filter

MIMO multiple-input multiple-output

ML maximum likelihood

MSE mean square error

OOB out-of-band

OFCDM orthogonal frequency and code division multiplexing

OFDM orthogonal frequency division multiplexing

OFDMA orthogonal frequency division multiplexing access

PA power amplifier

PAPR peak to average power ratio

PC personal computer

PEP peak envelope power

PMEPR peak-to-envelope power ratio

PTS partial phase sequence

QAM quadrature amplitude modulation

QPSK quadrature phase shift keying

RMS root mean square

SCs signal candidates

SC-FDMA single-carrier frequency-division multiple access

SI rside information

SLM selective mapping

SMS short message service

SNR signal to noise ratio

SPS sampling point selection

SSPA solid state power amplifier model

STO symbol time offset

TD-SLM time domain selective mapping

TDC-SLM time domain cyclic-selective mapping

TDMA time division multiple access

TDSC-CP time domain signal combining with cyclic delay and phase shift

TDSS time domain sequence superposition

TGn task group

UL uplink

UMTS universal mobile telecommunication system

UWB ultra wideband

VHT very higt throughput

WAP wireless aplication protocol

W-CDMA wideband-CDMA

WLAN wireless local area network

WiGig wireless gigabit alliance

WiMAX worldwide interoperability for microwave access

WPAN wireless personal network

List of Notations

A	clipping level
$B[k]$	PRT symbol
$b[n]$	time domain PRT symbol
$\mathbf{C}$	the sequence of split constellation
$C[n]$	average of delayed correlation output
$\hat{C}_m$	matched filter output
$\mathbf{C}^u$	conversion matrix
$c[n]$	delayed correlation output
$\hat{c}$	peak of delayed correlation output
$\tilde{\mathbf{D}}$	signal block of conversion metric
D	number of branches
$\hat{\Delta}$	cyclic shift estimation
Δ_d	amount of cyclic shift
Δ_f	frequency spacing between subcarriers
$\Delta^{\max}$	maximum peak of DC output
Δ_s	the interval of the peaks
δ	interval of cyclic shift
E_b/N_0	bit energy per noise
$\mathbf{F}$	$N \times N$ IDFT matrix
f_c	carrier frequency
G	index of the last non-zero element
$G[.]$	AM|AM conversion
g_0	amplifier gain
γ	average energy
γ_n	average energy per transmitted symbol
$\mathbf{H}$	channel matrix
$\hat{H}$	channel estimation response
$H_{e,m}$	channel frequency response
$H_p[m]$	pilot sub-channel response
$\hat{H}_p$	estimate pilot sub-channel response
$\mathbf{h}$	channel vector
$\hat{h}_d$	impulse response

$\mathbf{I}$	identity matrix
j	imaginary unit
K	subcarrier index
K_e	the extended symbol
L	the number of JROF
L_k	the length of the equivalent channel
L_p	the distance of two consecutive pilot symbols
M	number of OFDM symbols
N	number of subcarriers
N_d	number of data symbols
N_{GI}	length of guard interval
N_p	number of pilot symbols
N_v	number OFDM symbols sequence
N_0	noise spectrum density
n	discrete sampling index
$n^{\max}$	maximum amplitude of delayed correlation output
n_n	complex zero Gaussian
$\mathbf{P}$	phase vector factor
$\mathbf{P}_p^u$	phase factor of the pilot sequence
P_{av}	average power
$P_{\max}$	maximum power
p	the AM/AM sharpness controller of the saturation region
$\mathbf{P}$	phase vector factor
p^u	complex phase factor
$\Phi[.]$	AM|PM conversion
φ	phase factor for randomly distributed set over $[0, 2\pi)$
Q	number of received signal
Q_d	Barker sequences
θ_m	angle of arrival of the m^{th} clutter
$\mathbf{R}$	number of PRT symbol
$\mathbf{R}^b$	number of set PRT symbol
σ^2	variance of noise
σ_s	RMS value
$s[n]$	transmitted signal
$s_f[n]$	signal candidate
$S_{pre}[n]$	transmitted preamble signal
T	OFDM symbol duration
T_s	sampling interval
U	number of phase factor
$\tilde{u}$	SI index for transmission
$\hat{\tilde{u}}$	SI estimation
V	number of averaging symbols

$W[k]$	weighting coefficient of MMSE detection
$W_p[m]$	complex AWGN
$\tilde{W}$	set of phase factor
$\mathbf{w}$	zero-mean Gaussian random vector
$\mathbf{w}_q$	additive white Gaussian noise vector
w_k	rectangular window
$\mathbf{X}$	transmit OFDM symbol vector in frequency domain
$\mathbf{X}_q$	q^{th} transmit OFDM symbol vector in frequency domain
$\hat{\mathbf{X}}$	estimated symbol in frequency domain
$X[k]$	mapped signal on k^{th}
$X_p[2r]$	pilot symbol in frequency domain
$\hat{\mathbf{x}}$	estimated signal vector in time domain
$\mathbf{x}$	transmit signal vector in time domain
$x(t)$	transmit signal
$\tilde{x}(t)$	complex baseband signal
$x'[n]$	time domain signal before clipping process
x^u	signal candidates
$x^{\tilde{u}}$	the lowest PAPR of the SC
$x[n]$	n^{th} sample of $x(t)$
$x[n-\Delta]$	cyclically shifted signal
$x_d[n,\Delta_d]$	shifted signal
$x_f[n,\Delta]$	transmitted signal with GI
$x^p[n]$	the modulated signal with carrier frequency
$x_c^p[n]$	clipped signal
x_{sat}	the saturation level of PA
$\mathbf{Y}$	received vector
$Y[k]$	received signal in frequency domain
$Y_{pre}[n]$	received preamble signal
$\mathbf{y}_q$	q^{th} received OFDM signal vector
$y[n]$	received signal in time domain
$y_p[n]$	received preamble in time domain
$y_r[n]$	received signal for multiple branches in time domain
Z	power taps
$\lvert\cdot\rvert$	absolute value
$\{\cdot\}^*$	complex conjugate
$\lfloor\cdot\rfloor$	truncation operation
$\approx$	approximately equal to
$\{\cdot\}^H$	Hermitian transpose matrix
$\{\cdot\}^T$	transpose matrix
E[.]	ensemble average
$\odot$	multiplication of two vectors
$\otimes$	convolution

Abstract

Orthogonal frequency division multiplexing (OFDM) is a multicarrier transmission technique that has been recently adopted in many wireless communication standards. It has many advantages such as robustness to multipath fading and high spectrum efficiency. In spite of these advantages, OFDM suffers from its high peak-to-average power ratio (PAPR) signal which has become severe constraint in OFDM systems. The high PAPR may drive a power amplifier (PA) into a saturation region, cause interference among subcarriers, and corrupt the spectrum of the signal. In order to reduce the PAPR of the OFDM signal, many PAPR reduction schemes have been proposed and analyzed.

Time domain cyclic-selective mapping (TDC-SLM) has been proposed to reduce the PAPR. At the transmitter side, the signal candidates (SCs) are generated by summing the original signal and its cyclic delayed versions. The SCs with the lowest PAPR are chosen for transmission. The conventional TDC-SLM scheme requires sending the amounts of cyclic delays as side information (SI) at a receiver side. In this dissertation, cyclic delay estimation schemes at the receiver side are proposed. The proposed schemes omit the transmission of the SI and improve the throughputs of the OFDM systems by upto 10 %.

Chapter 1 introduces the OFDM concept and wireless communication standards, and the background of the research. The PAPR reduction schemes are then overviewed. The motivation of the research is represented in the last part of this chapter.

In Chapter 2 a delayed correlation (DC) estimation scheme for TDC-SLM at the receiver side is investigated. At the transmitter side, only one mapping branch is assumed and a SC with the lowest PAPR is applied. At the receiver, DC is used to estimate the cyclic delay. The DC process multiplies the received signal in the time domain with the conjugate of the guard interval (GI) sequence. The PAPR reduction, the bit error rate performance, and the accuracy rate of the estimation are evaluated under various channel conditions.

Chapter 3 proposes a DC-matched filtering (DC-MF) scheme that improves the DC estimation scheme in Chapter 2. The use of the MF makes the receiver be able to estimate the cyclic delays due to the generation of the SCs from multiple branches.

TDC-SLM places the DC-MF after the frequency domain equalization (FDE) to remove the multipath components of the received signal. This proposed scheme is also evaluated with the nonlinear PA.

Chapter 4 summarizes the results of each chapter and concludes this dissertation.

Chapter 1

Introduction

Over recent decades, the development of wireless technology occurs very rapidly. Millions of people share information every day in their personal or business activities using cell phones and the products of wireless communications. Therefore, the multimedia technology for wired and wireless links that support very high speed transmission rates, mobility, and spectrum efficiency. Orthogonal Frequency Division Multiplexing Systems (OFDM) is a multicarrier transmission technique that has been recently applied in many wireless communication standards such as asymmetric digital subscriber line (ADSL) services, wireless local area network (WLANs), digital audio broadcast (DAB), and digital terrestrial television broadcast. It has many well-known advantages such as robustness to multipath fading and high spectrum efficiency.

In spite of these advantages, OFDM suffers from its high peak-to-average power ratio (PAPR) signal which has become severe constraint in OFDM systems [1]. The very high peak of the transmitted signal leads to intermodulation among subcarriers due to the nonlinearity of devices. The high PAPR may drive a power amplifier (PA) into a saturation region, cause interference among subcarriers, and corrupt the spectrum of the signal. The high PAPR reduces the efficiency of the PA and degrades the performance of the system. Many PAPR reduction schemes have been proposed that can be classified into the following categories; distortion (clipping, filtering), distortionless selective mapping (SLM), partial transmission sequence (PTS), and coding (Hufman, Reed Muller) [1, 2].

In this chapter, wireless standards related to this thesis are introduced. The OFDM modulation scheme is explained, which is used in many wireless communication systems to achieve high data rate transmission. The motivation of the research is then presented.

1.1. Wireless Standards

1.1.1. Cellular Network

The first generation mobile phone uses multiple cell sites and the capability to handover from one site to another sites as mobile user during conversation was introduced [4]. In 1979, NTT Japan launched the first commercially automated cellular network (1G generations). This system was based on analogue modulation using around 900 MHz frequency range with frequency division multiple access (FDMA). A relatively small proportion of population had access to these systems. Some flaws with these systems were that they did not provide a great deal of security and standardization was not controlled particularly well.

Following the 1G, the second generation (2G) was commercially launched in 1991 [4]. The 2G systems were developed primarily for voice communications and incorporated with circuit-switching technology. In the past decade, some data communication capabilities have been added on with SMS (Short Message Service) and WAP (Wireless Application Protocol). Hence, these are quite limited in terms of functionality and available capacity. The popular 2G standards include time division multiple access (TDMA) and one code division multiple access (CDMA). Even though the 2G was the necessary revolution in the development of wireless communications, it has its limitations. Principally, the 2G wireless communications are classified as narrowband digital communications with the maximum data rate of 14.4 kbps [5]. Such a low data rate can not support real-time multimedia services as well as the wireless Internet access in high-mobility environments.

The 3G was designed for improved voice communications, the high-speed Internet, and multimedia services. The 3G network standards were drafted by International Telecommunication Union (ITU) and 3G universal mobile telecommunication system (UMTS) networks were developed under 3rd Generation partnership Project (3GPP) standards. Since 2001, NTT DoCoMo Corp. has launched the 3G service based on wideband-CDMA (W-CDMA). On the other hand, KDDI Corp. has started the service with CDMA2000 since 2002 [4]. Because many multimedia applications are packet oriented, it is essential to optimize the 3G system effectively for variable bit rate and packet based transmission. These systems purpose to support the wide distance of services varying from low rate voice transmission to high rate specifically, 2 Mbps for fixed environments, 384 kbps for pedestrian, and 144 kbps for vehicular traffic [4, 5].

High Speed Downlink Packet Access (HSDPA) is the 3.5G upgrade for existing W-CDMA networks. HSDPA is a packet-based data service in WCDMA downlink with data transmission up to 8-10 Mbps (and 20 Mbps for MIMO systems) over 5MHz bandwidth in a WCDMA downlink. On the other hand, CDMA2000 develops 1x evolution revision A data only (1xEV-DOrA) for the 3.5G and supports the downlink data rates

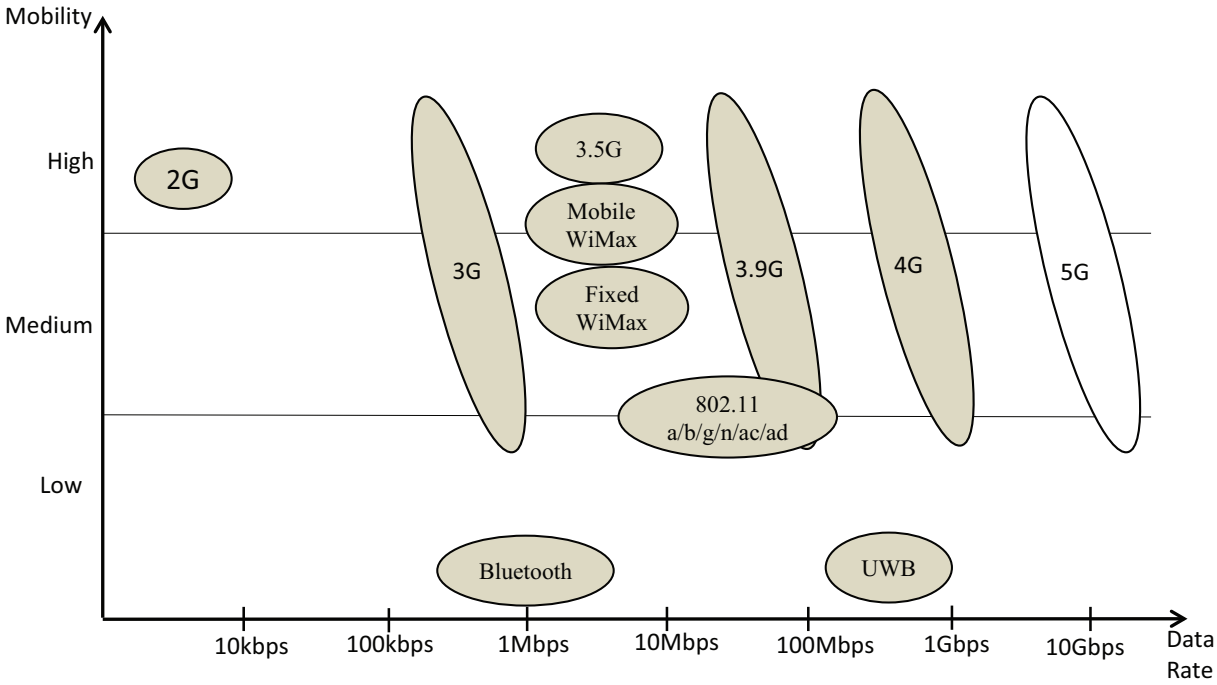

Figure 1.1: Wireless standards.

of up to 3 Mbps and the uplink rates of up to 1.8 Mbps.

The first version of LTE was completed in March 2009 as part of 3GPP Release-8 (Rel-8). LTE (Rel.8) depicted the future of the UMTS standard as it expands from an architecture that supports both circuit-switched and packet-switched communications to an all-IP, packet-only system. It is to serve high-data-rate, low-latency, offers flexible bandwidth options ranging from 1.4 MHz to 20 MHz, and also applies orthogonal frequency division multiple access (OFDMA) and single-carrier frequency division multiple access (SC-FDMA) as multiple access schemes in the downlink and the uplink, respectively. 3GPP LTE (4G) Release 10, LTE-Advanced, is expanded so as to meet the various requirements of advanced applications that support for heterogeneous deployments in order to fulfill and exceed the target set for future International Mobile Telecommunications-Advanced (IMT-A) 4G systems. The IMT-A also has capabilities for high-quality multimedia applications by providing significant improvement in the latency and the quality of the communication link. It is predicted that potential new radio interface(s) will need to support the data rates of up to approximately 100 Mbps for high mobility such as mobile access and up to approximately 1 Gbps for low mobility such as nomadic/local wireless access [6]. With the expansion of the wireless subscribers, various wireless standards have been developed for realizing an anywhere/anytime access network as shown in Fig. 1.1. The specifications of the cellular systems are shown in Table 1.1.

Table 1.1: Digital cellular communication systems.

Generation	2G	3G	3.5G	3.9G	4G
Name	GSM	IMT-2000		LTE	IMT-A
Frequency	900MHz	2GHz	2GHz	2GHz	3.4-3.6GHz
Rate	20kbps	2Mbps	14Mbps	100Mbps	1Gbps
Modulation	TDMA	W-CDMA	HSPA	DL:OFDM UL:SC-FDMA	OFDM, OFCDM

Table 1.2: WLAN Protocols

Protocol	Frequency	Rate	Modulation
IEEE 802.11a	5.2GHz	54 Mbps	OFDM
IEEE 802.11g	2.4GHz	54 Mbps	OFDM
IEEE 802.11b	2.4GHz	11 Mbps	DS / CCK
IEEE 802.11n	2.4GHz / 5GHz	600 Mbps	OFDM
IEEE 802.11ac	5GHz	6.93 Gbps	OFDM
IEEE 802.11ad	2.4GHz / 5GHz / 60GHz	6.76 Gbps	SC / OFDM

1.1.2. Wireless LAN

IEEE 802.11 WLAN standards had been developed originally as the replacement of a Ethernet cable [7]. However, WLAN terminals have penetrated into living rooms for the connections between electrical equipments such as personal computers (PCs), flat displays, video game platforms, and so on. As shown in Table 1.2, Wireless local area networks (WLANs) have been standardized in the IEEE 802.11 group such as IEEE 802.11a, 802.11b and 802.11g for the data rate of up to 54 Mbps [7]. In the IEEE 802.11a/g system, OFDM is used as a modulation scheme and the bandwidth per channel occupies 20 MHz in the 5 GHz and 2.4 GHz frequency bands, respectively. However, the transmission range is approximately 30m. On the other hand, the bandwidth per channel occupies 22 MHz in the 2.4 GHz frequency band using direct sequence spread spectrum (DSSS) and complementary code keying (CCK) in the IEEE.802.11b. Though the transmission range is approximately 100m, the data rate is about 11 Mbps.

Subsequently the IEEE 802.11n task group (TGn) began to develop an amendment to the IEEE 802.11 standard (i.e., IEEE 802.11n). Two basic concepts are employed in 802.11n to increase the PHY data rates: MIMO and 40 MHz bandwidth channels. According to [7, 8], 40 MHz bandwidth channel operation is optional in the standard due to concerns regarding interoperability between 20 and 40 MHz bandwidth devices, the permissibility of the use of 40 MHz bandwidth channels in the various regulatory

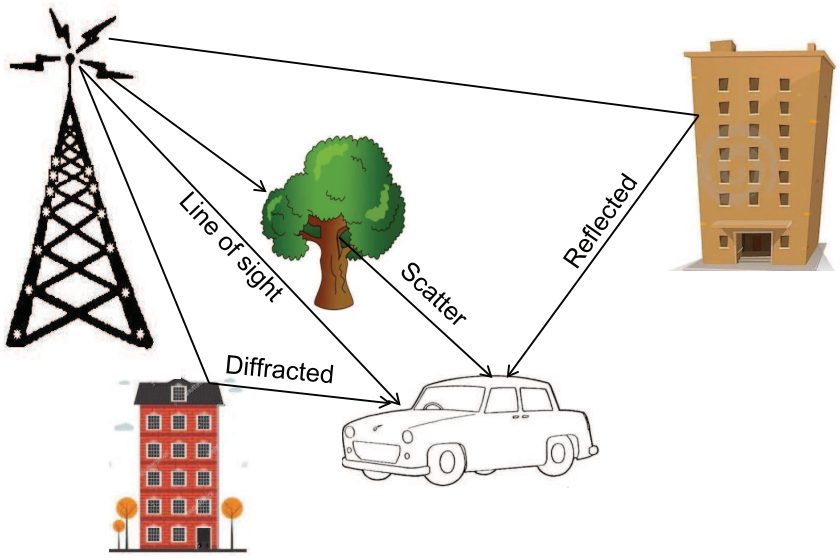

Figure 1.2: Multipath Fading.

domains, and spectral efficiency. With the PHY data rate of 600 Mbps, a media access control (MAC) throughput of over 400 Mbps is now achievable with 802.11n MAC enhancements. To cover the requirement of the high speed data transmission in 5G, WLAN standard proposed IEEE 802.11ac that operates in 5 GHz and has high speed data rate around 6.93 Gbps [9]. The IEEE 802.11ad standard was initially developed jointly with the Wireless Gigabit Alliance (WiGig) for packet based very high throughput (VHT) up to 6.76 Gbps communication over a short range using about 2 GHz of spectrum at 60 GHz [10].

1.2. Orthogonal Frequency Division Multiplexing Modulation

In a typical wireless communication environment, transmitted signals are reflected, diffracted and scattered separately by various obstacles as shown in Fig. 1.2 [11]. Then, these signals arrives at a receive antenna with different delays. This environment is called a multipath environment. The multipath environment causes serious distortion to a received signal. The multipath fading is typically modeled with Rayleigh distribution. It assumes that the amplitude of signal that has passed through such a transmission medium (also called a communication channel) vary randomly, or fade, according to Rayleigh distribution. Especially, the received signal spectrum is distorted in the wideband signal. This is a frequency-selective fading channel and it causes decoding error.

1.2.1. Multicarrier Principle

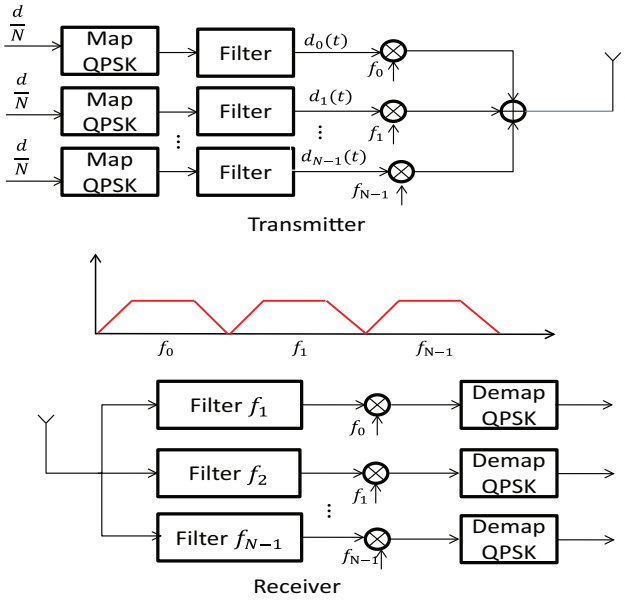

Figure 1.3: Block diagram of basic multicarrier system.

Since 1950's, multicarrier modulation schemes such as frequency division multiplexing (FDM) have existed and been developed to provide reliable high speed data transmission over wired and wireless channels [12]. Nevertheless, due to their implementation complexity and inefficient use of the frequency band they were limited to military applications. A multicarrier system is basically a number of information bearing carriers transmitted in parallel. Multicarrier systems in wireless applications are less susceptible to channel constrained distortions than single carrier systems at corresponding data rates. In the multicarrier modulation the data stream (d) is divided into (N) parallel data streams with a reduced data rate of $\frac{d}{N}$ as shown in Fig. 1.3. Each low rate data steam is then modulated on a separate narrow band subcarrier and all the modulation signals are summed together for transmission. Thereby it provides the same data rate as that of an equivalent single carrier system. The wideband signal is separated into the original narrowband subcarriers for demodulation in a receiver side. This scheme has disadvantage because the implementation complexity due to the large number of filter banks are needed in the transmitter and the receiver as well as the inefficient use of the available frequency band [13].

1.2.2. Overview of OFDM

OFDM was proposed as a special multicarrier modulation scheme [14]. OFDM has emerged as the key technology for supporting high data rate transmissions because of its high spectral efficiency and its robustnesss against multipath fading channels [15]. The basic principle of OFDM is to divide a stream of high-rate data into many of

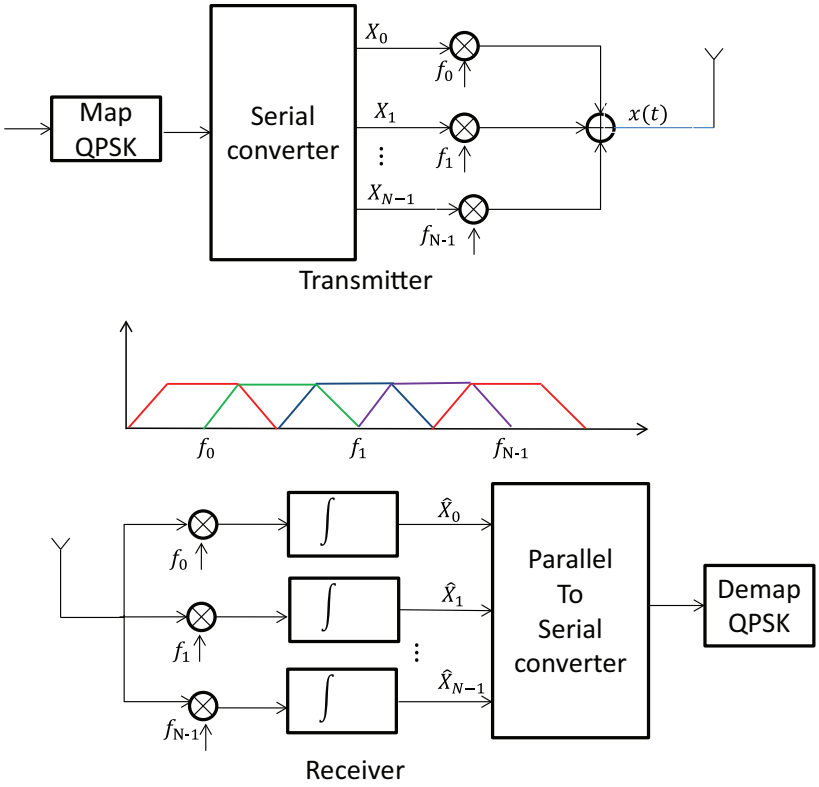

Figure 1.4: Block diagram OFDM.

parallel low-rate data streams which are mapped to a number of orthogonal subcarriers as shown in Fig 1.4. They are allowed to be overlaped and it utilizes the frequency spectrum much more efficiently. The OFDM transmitted signal is depicted as follow

$$x(t) = \frac{1}{\sqrt{N}} \sum_{\frac{-N}{2}+1}^{\frac{N}{2}} X_{m,k}\, e^{\left(j2\pi nk\Delta_f t\right)} w_k\left(t - mT\right),\ 0 \leqslant t \leqslant T, \tag{1.1}$$

where $X[k]$ is the mapped signal on the k^{th} subcarrier, Δ_f is the frequency spacing between subcarriers, T is the total time of the transmit symbol, and $w_k\left(t - mT\right)$ is a rectangular window for each subcarrier.

The discrete Fourier transform (DFT) and invers Fourier transmform (IDFT) are applied for baseband modulation to make multicarrier systems be more practical [13]. The discrete time representation of Eq. (1.1) can be obtained by sampling the continuous signal, under the condition of $\Delta_f = \frac{1}{T}$ and the signal can be determined by its samples with the interval of $\frac{nT}{N}$.

$$x[n] = \frac{1}{N} \sum_{k=0}^{N-1} X[k]\ \exp\left(j\frac{2\pi nk}{N}\right),\ 0 \leqslant n \leqslant N-1, \tag{1.2}$$

where n denotes the discrete sampling points. One of the significant advantages of OFDM is its efficient use of a frequency band since the subcarrier are allowed to be

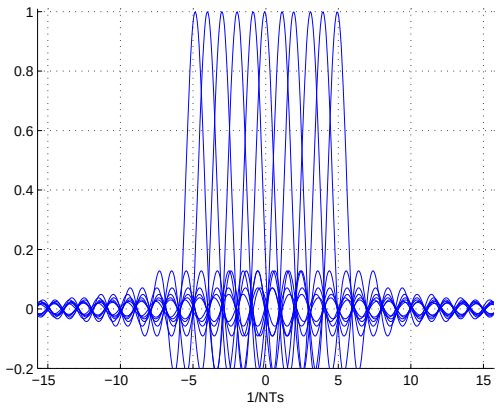

Figure 1.5: Frequency spectrum of OFDM.

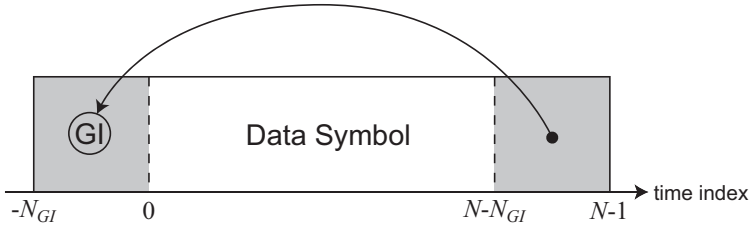

Figure 1.6: Cylic Prefix.

overlapped each other in a frequency domain as illustrated in Fig. 1.5. Therefore, the orthogonality between the OFDM subcarriers, the transmitted data is demodulated without introducing inter-carrier interference (ICI) in the receiver.

The OFDM systems add a guard interval (GI) to eliminate inter-symbol interference (ISI). The end of the symbol is copied and appended to the front before transmission and is removed at the receiver before the DFT operations as depicted in Fig. 1.6. Obviously the GI reduces the data throughput with a factor of

$$\frac{N}{N + N_{GI}}. \tag{1.3}$$

Hence, the length of the GI is desirable to be as short as possible.

The use of GI between consecutive OFDM symbols makes it immune to ISI. Also, it is less sensitive to sample timing offsets than single carrier system. The advantages of OFDM are given as [11]

- Saving of bandwidth

  OFDM systems are more bandwidth efficient in comparison to FDM. In the FDM technique numerous distinct carriers are spaced apart without overlapping while in OFDM the subcarriers overlap each other due to orthogonality feature. Because

of the overlapping of subcarriers the usage of bandwidth improves drastically and also the guard bands for the separation of subcarriers reduced.

- Ease of implementation.

  The challenging problem in a multi-carrier modulation (MCM) system is to implement a bank of modulators at the transmitter side and demodulators at the receiver side. The concept of data transmission can be efficiently implemented using IDFT and DFT instead of the modulators and the demodulations.

- Effectiveness of equalization

  In a single carrier system equalization makes the frequency spectrum of a signal flat. However, equalization amplifies noise greatly in a frequency domain when a frequency response is weak. As a result, the system performance is affected due to high attenuation in some bands since each frequency band is equalized with the same importance. In OFDM systems, the wideband channel is divided into flat fading sub-channels and it reduces the equalization complexity in the receiver. Thus, it is possible to use maximum likelihood decoding with reasonable complexity.

- Susceptible to frequency selective fading

  Due to the capability of parallel transmission (each subcarrier has narrow bandwidth as compared to the overall bandwidth of the signal) OFDM is highly susceptible to frequency selective fading. OFDM converts a frequency selective fading channel into several flat fading channels.

- Protection against Inter-symbol interference

  The extended symbol time (due to lower data rate) makes the signal less susceptible to the effect of the channel such as multipath propagation that introduces ISI. The use of cyclic prefix between consecutive OFDM symbols makes it immune to the ISI. Also, it is less sensitive to a sample timing offset than single carrier system.

However, OFDM has several major problems in spite of having been implemented in many communication systems.

- Synchronization (timing and frequency) at a receiver

  A symbol timing offset (STO) and a carrier frequency offset (CFO) effect on the performance of OFDM systems. Correct timing between DFT and IDFT is required at a receiver side. OFDM systems are highly sensitive to a Doppler shift that causes ICI.

- High PAPR of transmitted signal

  The particular problem of OFDM is high instantaneous signal peaks with respect to average signal power. Spurious high amplitude peaks in the continuous signal happens when the sinusoidal signals of the N subcarriers are summed constructively. The high PAPR is a challenge for a high power amplifier (HPA) at a transmitter. It will be driven into a saturation range unless the HPA is designed to operate over large dynamic ranges. The PAPR problem limits the usefulness of OFDM for various applications. Therefore, several schemes have been proposed to overcome this problem.

1.2.3. Nonlinear Power Amplifier

For the real implementation, HPA is applied before the transmission. Memoryless solid state amplifier (SSPA) is generally used fo OFDM systems. The input signal of the SSPA is describe as follows [16];

$$x(t) = |x(t)|e^{j\phi(t)}, \tag{1.4}$$

where $|x(t)|$ and $\phi(t)$ are the amplitude and phase of input signal, respectively. The HPA's output is given by

$$y(t) = G\left[|x(t)|\right] e^{j\{\phi(t)+\Phi[|x(t)|]\}}, \tag{1.5}$$

where $G[.]$ is AM|AM conversion and $\Phi[.]$ is AM/PM conversion. AM/PM for Rapp's models [17] as follow;

$$G[|x(t)|] = \frac{g_0|x(t)|}{\left[1+\left(\frac{|x(t)|}{x_{\text{sat}}}\right)^{2_p}\right]^{\frac{1}{2_p}}}, \tag{1.6}$$

where g_0 is the amplifier gain, x_{sat} is the saturation level of the PA, and p is a parameter that controls the AM/AM sharpness of the saturation region. Amplifier is nonlinear device, it is necessary to work in its linear region. The range of linear region of the PA is defined by input back-off (IBO). IBO is given by

$$\text{IBO} = 10\log\left\{\frac{x_{\text{sat}}^2}{\text{E}\left\{|x(t)|^2\right\}}\right\}, \tag{1.7}$$

where $E\left\{|x(t)|^2\right\}$ is the average of the input power. The IBO factor is defined as the ratio between the saturation power of PA and the average power of the input signal. The IBO is required to shift the operation point to the left as shown in Fig 1.7.

1.3. Peak-to-Average Power Ratio Reduction (PAPR) Schemes

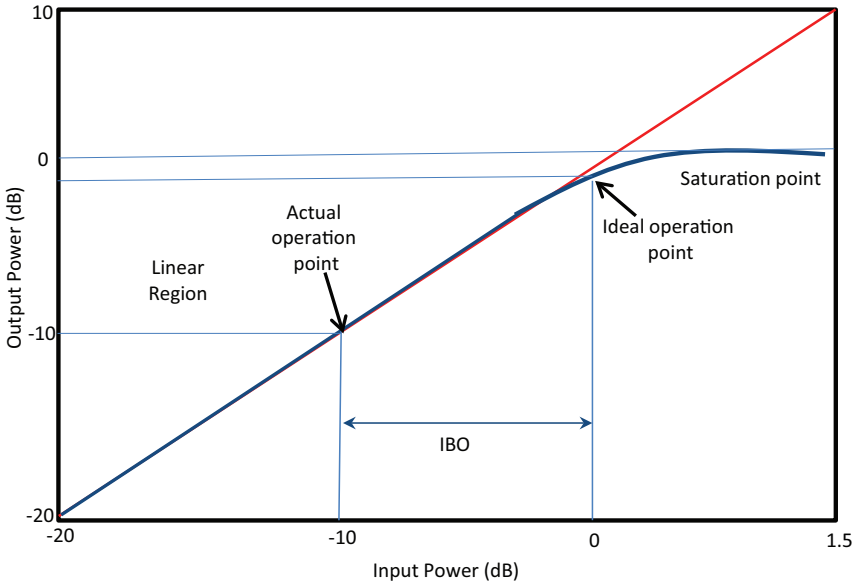

Figure 1.7: Typical input power vs output power for SSPA in dB.

One of the most important problems in OFDM is the PAPR of a transmit signal. The OFDM signal indicates large power variation with high infrequent peaks as compared to the average power as seen in Fig 1.8. The OFDM signal is composed of independently modulated subcarriers that may give a large PAPR when they are summed coherently. The peak power is defined as the power of a signal wave with an amplitude equal to the maximum envelope value. The peak-to-mean envelope power ratio (PMEPR) between the maximum power and the average power for the envelope of a complex baseband signal, $\tilde{x}(t)$, is expressed as follows;

$$\text{PMEPR}\{\tilde{x}(t)\} = \frac{|\tilde{x}(t)|^2}{\text{E}\{|\tilde{x}(t)|^2\}}. \tag{1.8}$$

The average power of the complex baseband signal is defined as

$$P_{av} = \text{E}\left[P\right] = \text{E}\left[|\tilde{x}(t)|^2\right]. \tag{1.9}$$

When the envelope of the OFDM signal is normalized (i.e., $E\{|\tilde{x}(t)|^2\}$), the peak envelope power (PEP) can be expressed as

$$\text{PEP}\{\tilde{x}(t)\} = \max|\tilde{x}(t)|^2. \tag{1.10}$$

The PAPR of the complex passband signal, $x(t)$, can then be defined as

$$\begin{aligned} \text{PAPR}\{\tilde{x}(t)\} &= \frac{\max\left|\text{Re}\left(\tilde{x}(t)e^{j2\pi f_c t}\right)\right|^2}{\text{E}\{\left|\text{Re}\left(\tilde{x}(t)e^{j2\pi f_c t}\right)\right|^2}\} \\ &= \frac{\max|x(t)|^2}{\text{E}\{|x(t)|^2\}}. \end{aligned} \tag{1.11}$$

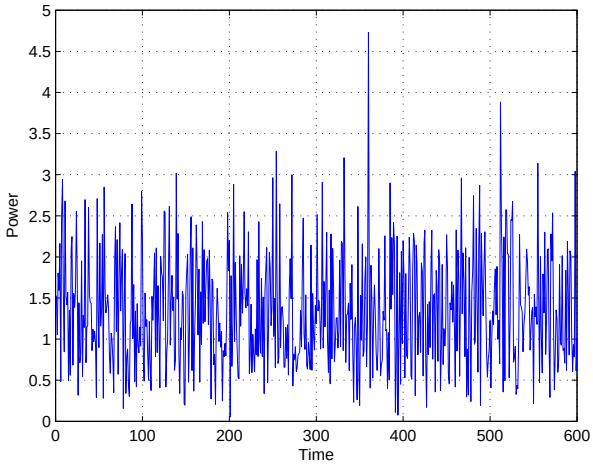

Figure 1.8: Power of OFDM Signal.

In practice, a more meaningful way to analyze the PAPR of the OFDM signal is to use the complementary cumulative distribution function (CCDF) [15]. The CCDF calculates the probability of the OFDM signal exceeding a specified PAPR threshold. The CCDF of the PAPR can be defined by

$$\begin{aligned}\left[\max_{0\leqslant n\leqslant N}\text{PAPR} > \text{PAPR}_0\right] &= 1 - P_r\left[\max_{0\leqslant n\leqslant N}\text{PAPR} \leqslant \text{PAPR}_0\right] \\ &= 1 - \left(P_r\left[\text{PAPR} \leqslant \text{PAPR}_0\right]\right)^N \\ &= 1 - \left(1 - e^{\text{PAPR}_0}\right)^N, \end{aligned} \tag{1.12}$$

where $\max_{0\leqslant n\leqslant N}\text{PAPR}$ is the crest factor.

PAPR reduction is classified into two categories

1. Frequency domain processing

   The high peaks occur when the summation of subchannels that generally have the same phase. The frequency domain processing attempts to interfere the complex input data to IDFT to reduce the occurrence of the peaks. One of the methods tries to change the phase of the complex data, the others try to change the power. In order to prevent bit error rate (BER) performance degradation, the phase adjustments should be relatively small [18]. Selective mapping (SLM), partial phase sequence (PTS) and random phase updating denote the frequency domain processing scheme for PAPR reduction. They generate some random phase factors to each modulation symbol to change the phase of the subcarriers. The frequency domain processing is divided into blind and non blind.

2. Time domain processing

In contrast to the frequency processing that attempts to avoid the occurrence of high peaks itself, the time domain processing tries to reduce high peaks that have already occurred. It applies after IDFT transformation. The time domain processing consists of blind and non blind. The simple blind scheme is clipping that cut the peak before the HPA. The clipping scheme is usually combine with filtering to reduce outbound radiation, though it results the peak regrowth [19]. The combining scheme is another blind time domain processing. It makes the signal with large amplitude variation into the uniformly distributed signal by compressing high peaks or by increasing the level of law signals.

There are several factors that should be considered to select the PAPR reduction scheme as well as can maintain the high quality performance [1–3] as follow

1. Without introducing in-band distortion and OOB radiation.
2. Low average power

   The raise in power requires a high linear operation region in PA and hence degres the BER performance.
3. No BER performance degradation

   The motivation of PAPR reduction is to get better system performance as well as BER than that of the original OFDM system.
4. Additional power

   Power efficiency should be considered while reducing the PAPR. If the scheme requires more additional power, it decreases the BER performance when the transmitted signals are normalized back to the original power signal.
5. No spectral spillage

   The PAPR reduction scheme should not destroy the inherent feature (orthogonality) of OFDM signal.

1.3.1. Clipping and Filtering

The simplest PAPR reduction scheme is clipping in which the peak values above a specified threshold in the time domain is removed [20–22]. The block diagram of the clipping and filtering scheme can be seen in Fig. 1.9. The time domain signal, $x'[n]$, is generated from the IDFT block and then modulated with carrier frequency, f_c, to get $x^p[n]$. The clipped signal, $x_c^p[n]$, is expressed as

$$x_c^p[n] = \begin{cases} x^p[n] & \text{if } |x^p[n]| < A \\ \frac{x^p[n]}{|x^p[n]|} & A \quad \text{otherwise,} \end{cases} \tag{1.13}$$

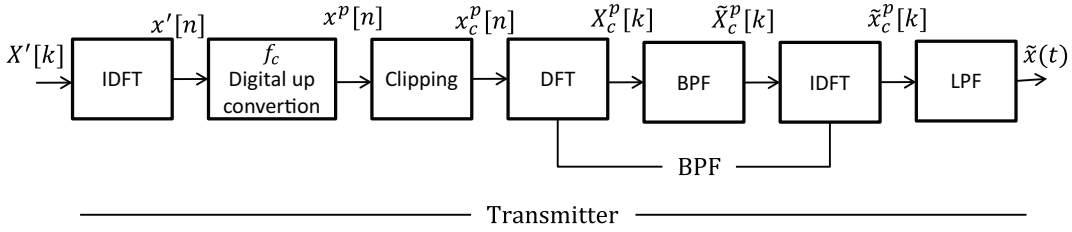

Figure 1.9: Block Diagram PAPR reduction by Using Clipping and Filtering.

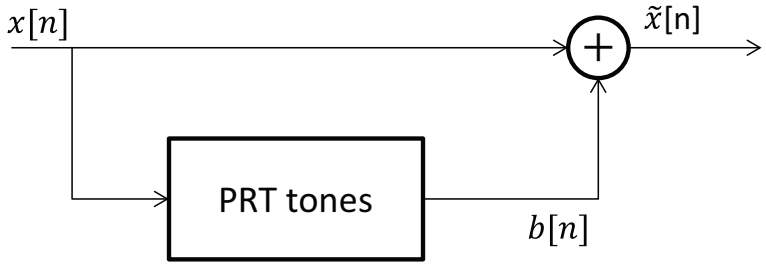

Figure 1.10: PAPR Reduction by Using Tone Reservation.

where $A = CR * \sqrt{\sigma}_s$, A is the clipping level, and clipping ratio (CR) is the clipping level normalized by the root mean square (RMS) value, σ_s, of the OFDM signal. The clipping and filtering scheme has disadvantages as follows;

1. Performance degradation

   The clipping and filtering cause in band signal distortion that leads to BER performance degradation.

2. Out-of-band (OOB) distortion

   It decreases the spectral efficiency of an OFDM system and interference to adjacent channels [20].

3. Peak regrowth

   The OOB signal at a clipping can be reduced by filtering. However, the signal after filtering process may exceed the clipping level specified for clipping operation.

1.3.2. Tone Reservation

Tone reservation (TR) uses tones to reduce the high PAPR of the OFDM signal as shown in Fig. 1.10. In the TR scheme, $\mathbf{R}$ peak reduction tones (PRTs), $B[k]$, is added to the original signal [15, 20].

$$X[k] + B[k] = \begin{cases} X[k], & k \in \mathbf{R} \\ B[k], & k \in \mathbf{R}^b, \end{cases} \tag{1.14}$$

where $\mathbf{R}$ denotes the index set of data-bearing subcarriers and $\mathbf{R}^b$ is the set of $\mathbf{R}$ PRT positions, $X[k]$ is the data symbol and $B[k]$ denotes the PRT symbol on the k^{th} subcarrier. The corresponding time domain signal is obtained as follows;

$$x[n] + b[n] = \frac{1}{N} \sum_{k=\mathbf{R}^b} \left(X[k] + B[k]\right) e^{j2\pi kn/N}. \tag{1.15}$$

In the TR, the PRTs will consume the transmit power and decrease the data rate because the location of the PRT tones require to be known by a receiver. Consequently, they are transmitted as overhead information [23].

1.3.3. Partial Phase Sequence

In PTS scheme, the frequency domain symbol sequence, $\{X[k]\}$, is partitioned into several subblocks, U, as follows [24, 25].

$$\mathbf{X} = \left[\mathbf{X}^0, \mathbf{X}^1, \mathbf{X}^2 ..., \mathbf{X}^{U-1}\right]^T, \tag{1.16}$$

where $\mathbf{X}^i$ is the subblock that are consecutively located and also are the equal size. The scrambling (rotating its phase independently) is applied to each subblock in the PTS scheme as shown in Fig. 1.11. The corresponding complex phase factor $p^u = e^{j\varphi u} (u = 1, 2, ..., U)$ is multiplied with each partition subblock [24, 26]. Subsequently taking its IDFT generates

$$\mathbf{x} = \text{IDFT}\left\{\sum_{u=1}^{U} p^u \mathbf{X}^u\right\} = \sum_{u=1}^{U} p^u \text{IDFT}\left\{\mathbf{X}^u\right\} = \sum_{u=1}^{U} p^u \mathbf{x}^u \tag{1.17}$$

where $\{\mathbf{x}^u\}$ is referred to as a partial transmit sequence (PTS). In order to minimize the PAPR, the phase vector is selected as follows;

$$\left[\tilde{p}^1, ..., \tilde{p}^U\right] = \arg \min_{[p^1, ..., p^U]} \left(\max_{n=0,1,...,N-1} \left| \sum_{u=1}^{U} p^u x^u[n] \right| \right). \tag{1.18}$$

The lowest PAPR vector can be described as

$$\tilde{\mathbf{x}} = \sum_{u=1}^{U} \tilde{p}^u \mathbf{x}^u. \tag{1.19}$$

$\mathbf{p} = \left\{ e^{2i\pi/\tilde{W}} | i = 0, 1, ..., \tilde{W} - 1 \right\}$ is the set of phase factors that changes the phase of the signal vector in the time domain and the optimum set of the phase factor is found from $\tilde{W}^{U-1}$ sets of the phase factors. U IDFT operations and $\{\log_2 \tilde{W}^U\}$ bits of the side information (SI) are needed for each data block in the PTS scheme. The amount of PAPR reduction depends on U and $\tilde{W}$. The greater PAPR reduction is occurred when the number of data blocks, U, increases while the complexity also increases exponentially with U.

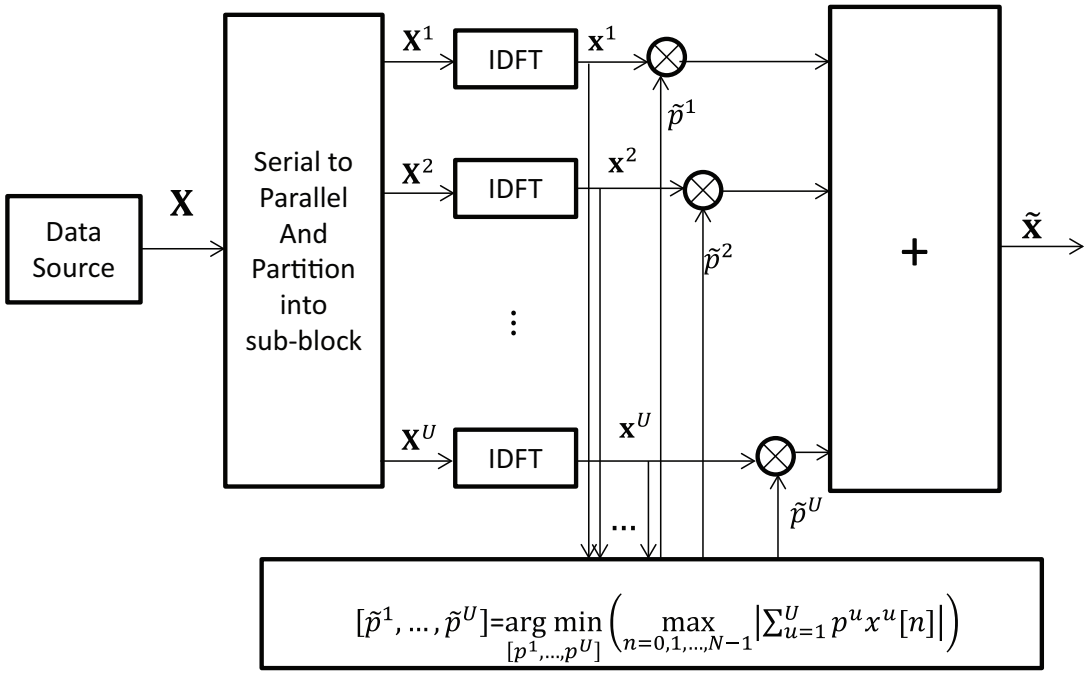

Figure 1.11: Partial Phase Sequence.

1.3.4. Selective Mapping

Selective mapping (SLM) is a popular PAPR reduction scheme. The basic idea of the SLM scheme is based on phase rotation [27, 28]. The phase rotation is used to generate U statistically independent OFDM symbols shown in Fig. 1.12. The OFDM symbols, $\mathbf{X}$, are multiplied with the different phase factor, $\{ \mathbf{P}^u = [P_0^u, P_1^u, ...P_{N-1}^u)] \}$, where $P_i^u = e^{j\varphi_i^u}$, $\varphi_i^u \in [0, 2\pi)$ for $i = 0, 1, ..., N-1$, and $u = 1, 2, ..., U$.

$$\begin{aligned} \mathbf{X}^u &= [X^u(0), ...X^u(N-1)] \\ &= \mathbf{X} \odot \mathbf{P}^u \\ &= \left[\bar{X}(0)P^u(0), ..., \bar{X}(N-1)P^u(N-1)\right], \quad 1 \leqslant u \leqslant U, \end{aligned} \tag{1.20}$$

where $\odot$ is the component-wise multiplication of the two vectors. The resultant vector is then input into the IDFT block as

$$\mathbf{x}^u = \text{IDFT}\left(\mathbf{X} \odot \mathbf{P}^u\right), 1 \leqslant u \leqslant U. \tag{1.21}$$

Then, the PAPR of these U vectors are calculated separately and the lowest PAPR among the signal candidates (SCs), $\tilde{\mathbf{x}} = \mathbf{x}^{\tilde{u}}$, is chosen for transmission, which is given as

$$\tilde{u} = \arg \min_{u=0,2,\dots,U-1} \left(\max_{n=0,1,\dots,N-1} |x^u[n]| \right). \tag{1.22}$$

The SLM scheme requires U times of the IDFT and $\{\log_2 U\}$ bits of the SI for each

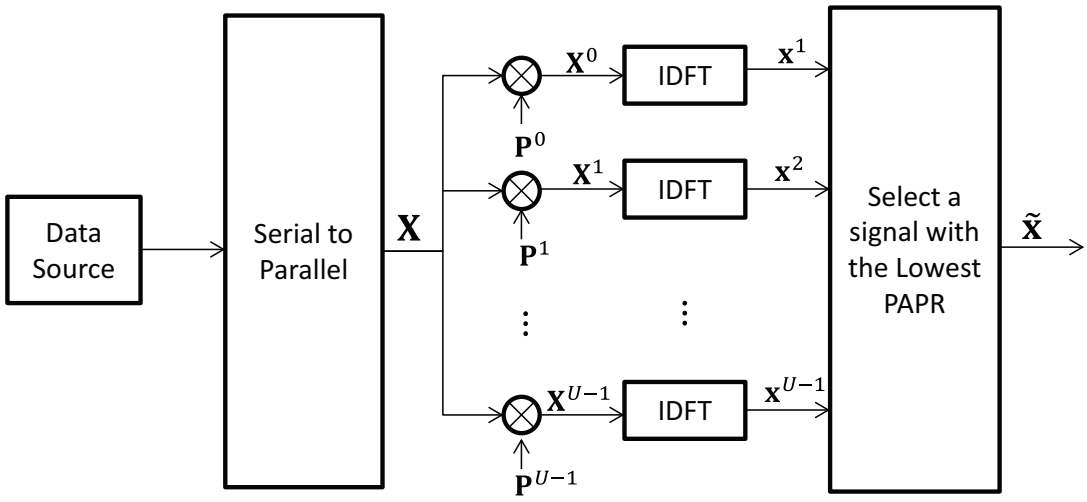

Figure 1.12: Conventional SLM.

block. The number and the design of the phase sequences are effected to the amount of PAPR reduction.

1.3.5. Time Domain Cylic Selective Mapping

The time domain SLM (TD-SLM) has been proposed to reduce the computational complexity of the frequency domain (FD-SLM). The TD-SLM tries to change the power in the time domain so that it less computational complexity than the FD-SLM. The low complexity SLM (LC-SLM) is based on TD-SLM. It was designed to use only one or two IDFT operation [29–31] and the SCs are obtained by multiplying the time-domain signal to the conversion matrices. The time domain cyclic selective mapping (TDC-SLM) was introduced in [32]. It combines the OFDM signal with its cyclically delayed in the time domain to get the lowest PAPR for transmission. In this scheme possesses half computational complexity than LC-SLM at similar PAPR and BER performance. The TDC-SLM can be described in Fig. 1.13.

The cyclically shifted signal, $x_c[n, \Delta]$, of the TDC-SLM in the time domain are given as

$$x_c[n, \Delta] = \begin{cases} x[N - \Delta + n], & 0 \leqslant n \leqslant \Delta - 1 \\ x[n - \Delta], & \Delta \leqslant n \leqslant N - 1, \end{cases} \tag{1.23}$$

where Δ is the amount of the cyclic shift. The SCs, $s_f[n]$, are the summation of the original signal and its cyclically shifted signal in the time domain as follows

$$s_f[n] = x_f[n] + x_f[n, \Delta], \tag{1.24}$$

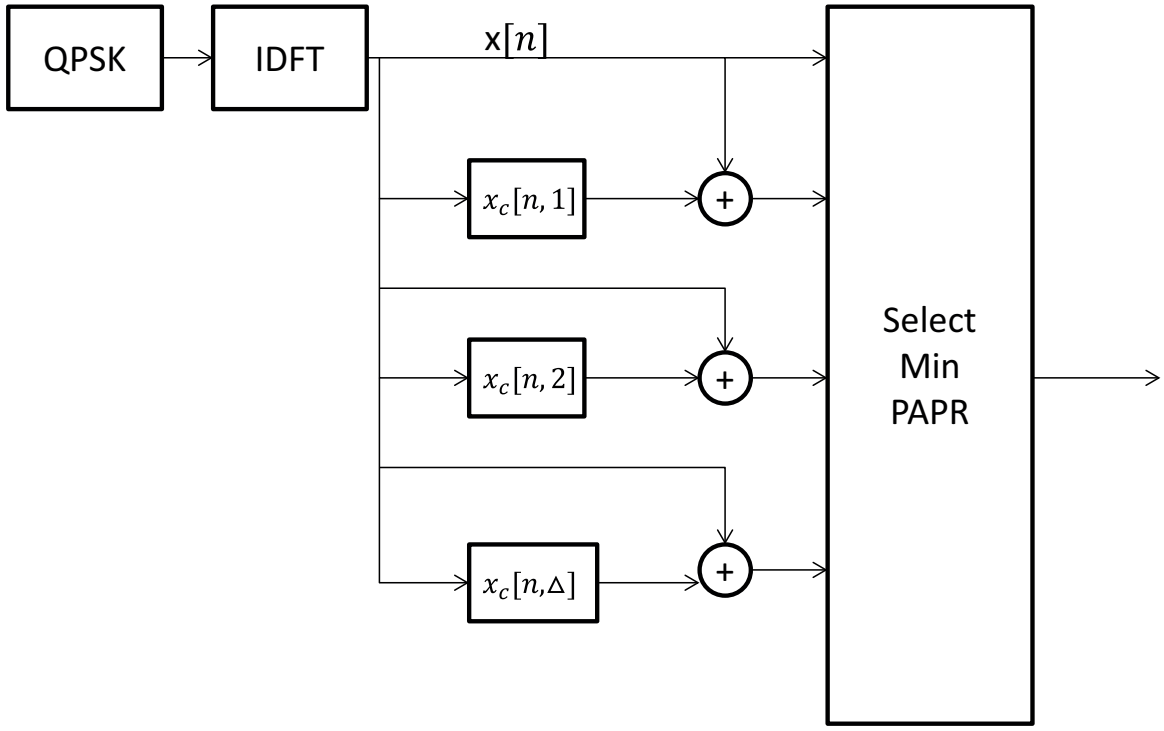

Figure 1.13: TDC-SLM.

where $x_f[n,\Delta]$ denotes the cyclically shifted signal with the GI, which is given as

$$x_f[n,\Delta] = \begin{cases} x_c[n,\Delta], & 0 \leqslant n \leqslant N-1 \\ x_c[N+n,\Delta], & -N_{GI} \leqslant n < 0, \end{cases} \tag{1.25}$$

where $0 < \Delta < N - N_{GI}$. After summing the original signal and its cyclically shifted signal in Eq. (1.24), the SC that achieves the lowest PAPR is selected as the transmitted signal, $s[n]$.

1.4. Side Information Detection

The most of SLM schemes assume that the SI is sent through the dedicated channel in order to help the receiver demodulated the received signal. The SI transmission is not a simple task since it is sent together with an OFDM signal. It effects on the spectrum efficiency and causes throughput degradation. Many SI detection schemes have been proposed to avoid SI transmission.

1.4.1. Conversion Matrices

A novel set of conversion matrices (CMs), $\mathbf{C}_i$, has been proposed in [33] to avoid the SI transmission. The u^{th} candidate signal in Eq. (1.21) can be written as follows;

$$\tilde{\mathbf{x}}_q^u = \mathbf{F}\mathbf{X}_q^u = \mathbf{p}^u \otimes \mathbf{x}_q = \mathbf{C}^u \mathbf{x}_q, \tag{1.26}$$

where $\mathbf{F}$ is the $N \times N$ IDFT matrix, $\mathbf{p}^u = \mathbf{F}\mathbf{P}^u$, $\mathbf{x}_q = \mathbf{F}\mathbf{X}_q$, $\mathbf{P}^u$ is the phase rotation vector, $\mathbf{X}_q$ denotes the q^{th} OFDM symbol in the frequency domain, and the circulant matrix $\mathbf{C}^u = \left[\mathbf{p}_1^u, \mathbf{p}_2^u, ..., \mathbf{p}_{N-1}^u\right]$ is refered to as the CM. The CMs have a special structure for a block of an OFDM signal, with which the equivalent channel coefficient of the wireless channel combined with the phase rotation vector can be estimated by the finite number of pilots in the block. There are four restrictions on the first column vector, $\mathbf{p}^u = \mathbf{F}\mathbf{P}^u$, of $\mathbf{C}^u$ [33]:

1. The few nonzero elements of $\mathbf{p}^u$ are concentrated in the front of it to decrease the length of the equivalent channel vector.

2. The first column vector $\mathbf{p}^u = \mathbf{F}\mathbf{P}^u$ of $\mathbf{C}^u$ has K nonzero elements, where $K = 3$ or 4.

3. To maintain the power constraint, the module of $\mathbf{p}^u$ is normalized.

4. The frequency response $\mathbf{P}^u$ of the vector $\mathbf{p}^u$ has no significant nulls.

After removing GI, the q^{th} received OFDM signal vector can be expressed as

$$\mathbf{y}_q = \mathbf{h} \otimes \tilde{\mathbf{x}}_q + \mathbf{w}_q, 1 \leqslant q \leqslant Q, \tag{1.27}$$

where $\mathbf{w}_q$ is the additive white Gaussian noise vector to the u^{th} received OFDM signal vector. If $\mathbf{p}^u$ is the first column vector of $\mathbf{C}^u$ that minimizes the PAPR of the signal block $\tilde{\mathbf{D}} = [\mathbf{x}_1, ..., \mathbf{x}_q, ..., \mathbf{x}_Q]$, Eq. (1.27) can be written as

$$\mathbf{y}_q = \mathbf{h} \otimes \tilde{\mathbf{x}}_q + \mathbf{w}_q = \mathbf{h} \otimes \mathbf{p}^u \otimes \mathbf{x}_q + \mathbf{w}_q, \quad 1 \leqslant q \leqslant Q, \tag{1.28}$$

where the equivalent channel vector is defined as $\mathbf{h}_e = \mathbf{h} \otimes \mathbf{p}^u$ then

$$\mathbf{y}_q = \mathbf{h}_e \otimes \mathbf{x}_q + \mathbf{w}_q, \qquad 1 \leqslant q \leqslant Q. \tag{1.29}$$

Let $\mathbf{h}_e = \left[h_{e,0}, ..., h_{e,L_k'-1}\right]^T$, where L_k' is the length of the equivalent channel. After taking the DFT of $\mathbf{y}_q$, the $m^{\mathbf{th}}$ component of that is given as

$$Y_q^m = H_{e,m} X_q^m + W_q^m, \qquad 0 \leqslant m \leqslant N, \tag{1.30}$$

where $H_{e,m} = H_m P^u = \sum_{l_k=0}^{L_k'-1} h_{e,l_k} e^{j\frac{2\pi m l_k}{N}}$ is the equivalent channel frequency response. Since $\mathbf{h}_e = \mathbf{h} \otimes \mathbf{p}^u$, $L_k' = L_k + G - 1$ is easy to be found where G is index of the last non-zero element of $\mathbf{p}^u$, and L_k is the number of the taps of the wireless channel [33]. Because of the small value of G, L_k' is much smaller than the number of pilots in OFDM. The equivalent channel coefficient can be estimated and the weighted factor on each subcarrier is removed in the equalization process so that the signal can be recovered at receiver without SI.

This scheme has disadvantage in recovery signal at the receiver side because the pilot subcarriers is required to estimate the frequency response of the channel. Moreover, there are several constraints to establish the block of OFDM symbols that are related to the length of the correlated channel response and the number of non-zero elements.

1.4.2. Maximum Likelihood Detection

In [34] the TDC-SLM scheme is used at the transmitter. It only requires single IDFT to generate the SCs in the time domain. The output symbol of IDFT is multiplied with in-phase and quadrature recombination (IQRC) block where the total number of IQRC is $U(u = 1, 2, ..., U)$. IQRC consists of multiple subunit dubbed joint rotation and offset (JROF) and each IQRC has L JROFs, $(L \times U + 1)$ SCs are generated, the SC with the minimum PAPR is chosen to be transmitted. Maximum likelihood (ML) detection is used to demodulate the receive signal without the SI. The ML detection metric for the source symbol is given by

$$\min_{\hat{l}\in L, \hat{u}\in U, \tilde{\mathbf{X}}\in \mathbf{C}} \|\tilde{\mathbf{Y}} - \tilde{\mathbf{H}}\mathbf{F}_l^u \tilde{\mathbf{X}}\|, \tag{1.31}$$

where $\tilde{\mathbf{Y}} = [\mathrm{Re}(\mathbf{Y})^{\mathrm{T}} \mathrm{Im}(\mathbf{Y})^{\mathrm{T}}]^{\mathrm{T}}$, $\mathbf{Y}$ is the received signal, $\tilde{\mathbf{H}}$ is the channel matrix, $\tilde{\mathbf{X}}$ is a split vector of transmit signal $\begin{bmatrix} \mathbf{Re(X)} \\ \mathbf{Im(X)} \end{bmatrix}$, $\mathbf{F}_l^u$ is a precoding matrix for the vector of $\tilde{\mathbf{X}}$, $\mathbf{C} = \{c_0, c_1, ..., c_{2N-1}\}$ is the sequence of split constellation, $\hat{l}, \hat{u}$, and $\hat{\mathbf{X}}$ are l, u and $\tilde{\mathbf{X}}$ that minimize the ML metric, respectively.

$$\min_{\hat{l}\in L, \hat{u}\in U} \sum_{i=0}^{N/2-1} \min_{\hat{\mathbf{X}}_{\mathbf{\Psi}_i} \in \mathbf{C}_{\mathbf{\Psi}_i}} \|\mathbf{Y}_{\mathbf{\Psi}_i} - \tilde{\mathbf{H}}_{\mathbf{\Psi}_i} \mathbf{F}_{l,\mathbf{\Psi}_i}^{(u)} \tilde{\mathbf{X}}_{\mathbf{\Psi}_i}\|, \tag{1.32}$$

where Ψ_i, for $i = 0, 1, ..., \frac{N}{2} - 1$, is a set of indices that satisfy the following condition.

$$\mathbf{\Psi}_i = \begin{cases} \{(k,k)|k = i, N-i, N+i, 2N-i\}, & 1 \leqslant i \leqslant \frac{N}{2} - 1 \\ \{(k,k)|k = i, N+i\}, & i = 0, \end{cases} \tag{1.33}$$

for matrices or

$$\mathbf{\Psi}_i = \begin{cases} \{k|k = i, N-i, N+i, 2N-i\}, & 1 \leqslant i \leqslant \frac{N}{2} - 1 \\ \{k|k = i, N+i\}, & i = 0, \end{cases} \tag{1.34}$$

for both vectors and sequences. The ML detector structure can be seen in Fig. 1.14. The SI, $\hat{l}$ and $\hat{\mathbf{X}}$ are minimizing the ML metric l and $\tilde{\mathbf{X}}$, respectively, that can found by Eq. (1.32). The ML detection scheme still has computational complexity in the receiver side.

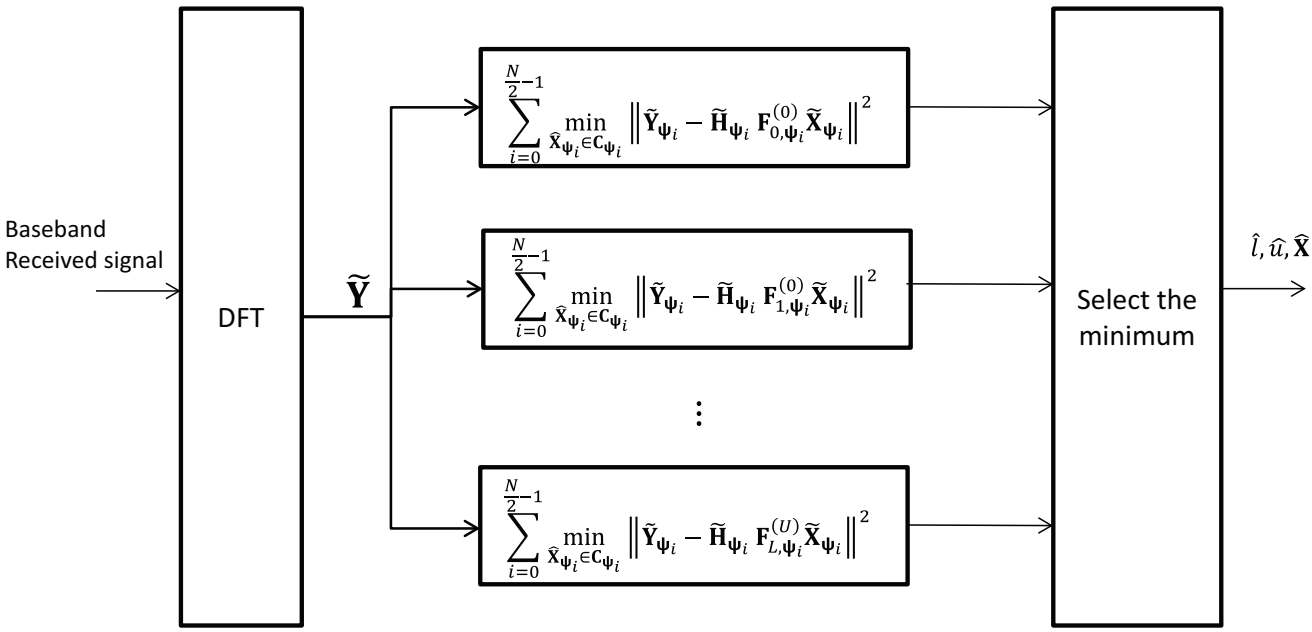

Figure 1.14: ML Detector for Transmitted Source Symbol.

1.4.3. Energy Detection

The SI is estimated by the average difference between K_e extended symbols and the $(N - K_e)$ non extended symbols in vector $\mathbf{X}^{\tilde{u}} = (x^{\tilde{u}}[n])_N$ with $x^{\tilde{u}}[n] = p^{\tilde{u}}[n]x[n]$ [35]. $\mathbf{X} = (x[n])_N$ is a data block that composed of N complex symbols, $x[n]$. The index $\tilde{u}$ describes the SI index to be transmitted. The received sample in the frequency domain, $y[n]$, corresponding to the n^{th} subcarrier is given as

$$y[n] = h[n]x^{\tilde{u}}[n] + w[n], \tag{1.35}$$

where

$$h[n] = \sum_{z=0}^{Z-1} \grave{h}_z e^{\frac{-i2\pi nz}{N}}, \tag{1.36}$$

$w[n]$ denotes a complex zero-mean Gaussian noise sample with variance $\sigma^2 = N_o$, and Z is equal power taps. The receiver selects the SI index by using ML detection that minimizes the term

$$\sum_{n=0}^{N-1} \left| y[n] - h[n]p^u[n]x[n] \right|^2, \qquad u \in \{0, 1, ..., U-1\}. \tag{1.37}$$

The average received energy at the location of n without additive noise would be given

by

$$\mathrm{E}\left\{|h[n]|^2|x^u[n]|^2\right\} = |h[n]|^2|p^u[n]|^2\gamma, \tag{1.38}$$

where γ is the average energy per complex symbol $x[n]$. The average energy of the received sample, $y[n]$, is given by

$$\mathrm{E}\left\{|y[n]|^2\right\} = |h[n]|^2|p[n]^{\tilde{u}}|^2\gamma + \sigma^2. \tag{1.39}$$

A metric $\alpha^u[n]$ is expressed as

$$\alpha^u[n] = \left|\mathrm{E}\left\{|y[n]|^2\right\} - \sigma^2 - |h[n]|^2|p[n]^{\tilde{u}}|^2\gamma\right|. \tag{1.40}$$

By using Eq. (1.39), Eq. (1.40) can be written as

$$\alpha^u[n] = |h[n]|^2\gamma\left||p[n]^{\tilde{u}}|^2 - |p[n]^u|^2\right|. \tag{1.41}$$

The metric β^u is extending a particular location n of the whole received vector as follows;

$$\beta^u = \left|\sum_{n=0}^{N-1}\alpha^u[n]\right|. \tag{1.42}$$

The minimal value of the metrics $\alpha[n]^u$ and β^u are equal to 0 when $|p^u[n]| = |p^{\tilde{u}}[n]|$ is satisfied for all values of n, i.e $P^{\tilde{u}} = P^u$ or equivalent $\tilde{u} = u$. The SI index is estimated by determining the values of u that minimizes the metric β^u. In this scheme, the SI detection error is effected by higher order modulation.

1.4.4. Suboptimal Side Information

Suboptimal SI detection is based on the ML detection algorithm [35]. After the DFT process, the corresponding transformed received vector is $\mathbf{Y} = \{y[n]\}_{n=0}^{N-1}$ and $y[n] = h[n]x^u[n] + n[n]$. The SI index $\tilde{u}$ minimizes Eq. (1.37) which is less than or equal to [36];

$$\begin{aligned} & \sum_{n=0}^{N-1}\left||y[n]|^2 - 2\left|y[n]h[n]p^u[n]x[n]\right| + \left|h[n]p^u[n]x[n]\right|^2\right| \\ = & \sum_{n=0}^{N-1}\left||y[n]|^2 - 2\left|n[n]h[n]p^u[n]x[n]\right| - \left|h[n]p^u[n]x[n]\right|^2\right|. \end{aligned} \tag{1.43}$$

By applying expectation, the middle term $\mathrm{E}\{n[n]h[n]p^u[n]x[n]\}$ vanishes because the transmitted symbols $x[n]$ and noise are uncorrelated. The suboptimal SI receiver chooses the SI index, u, that gives the minimal value of α^u, as the received SI index $\tilde{u}$,

$$\alpha^u[n] = \sum_{n=0}^{N-1}\left||y[n]|^2 - |h[n]|^2|p^u[n]|^2\gamma[n]\right|, \tag{1.44}$$

where $\gamma[n]$ is equal to γ the average energy per transmitted symbol $x[n]$ for low symbol energy to noise ratio while for high symbol energy to noise ratio $\gamma[n]$ is an estimate of $|x[n]|^2$. γ and the estimate of $|x[n]|^2$ are different only in modulation that has different energies for its modulated symbols like QAM modulation techniques. In this scheme, the possible phase vector is prepared in the receiver side.

1.4.5. Pilot Sequence Detection

The N_v OFDM symbol sequence, $\{X[k]\}$, are divided into N_d data symbols, $X_d[mL_p+l_p]$, and N_p pilot symbols, $X_p[m]$, as given in the following equation [37].

$$X\left[k\right]=X\left[mL_p+l_p\right]=\begin{cases} X_p\left[m\right], & l_p=0 \\ X_d\left[mL_p+l_p\right], & l_p=1,2,...,L_p-1, \end{cases} \tag{1.45}$$

where L_p is the distance of two consecutive pilot symbols, m and l_p are the quotient and remainder of $\frac{k}{L_p}$ respectively. The phase sequence $\mathbf{P}^u$ is divided to pilot sequence, $\{P_p^u[m]\}$, and data phase sequence

$$P_p^u[m]=\begin{cases} 1, & m=2r \\ e^{j\varphi^u[m]}, & m=2r+1 \end{cases} \tag{1.46}$$

where $0\leqslant r\leqslant\lfloor(N_p/2)-1\rfloor$ and $\lfloor.\rfloor$ is a truncation operation and $\varphi^u[m]$ is obtained from a randomly distributed set over $[0,2\pi)$. The received pilot sequence, $Y_p[m]$, after through the DFT can be given as follows;

$$Y_p[m]=H_p[m]P_p^{\tilde{u}}[m]X_p[m]+W_p[m] \tag{1.47}$$

where $\{P_p^{\tilde{u}}[m]\}$ is the selected pilot phase sequence, $H_p[m]$ is the pilot sub-channel response and $W_p[m]$ is the complex AWGN. The pilot sub-channel response of the even index, $\hat{H}_p[2r]$, is estimated as following

$$\hat{H}_p[2r]=Y_p[2r]/X_p[2r]=H_p[2r]+W_{X_p}[2r] \tag{1.48}$$

where $X_p[2r]$ and $W_{X_p}[2r]$ denote the pilot symbols and another complex AWGN sequence, respectively. By a simple linear interpolation between $\hat{H}_p[2r]$ and $\hat{H}_p[2r+2]$, the estimated pilot sub-channel response of the odd index, $\hat{H}_p[2r+1]$, is represented as

$$\hat{H}_p[2r+1]=\left(\hat{H}_p[2r]+\hat{H}_p[2r+2]\right)/2 \tag{1.49}$$

The ML detection estimates the SI on the pilot sub-channel response as follows;

$$\hat{\tilde{u}}=\arg\min_{u\in\{0,1,...,U-1\}}\sum_{r=0}^{\lfloor\frac{N_p}{2}-1\rfloor}\left|Y_p[2r+1]-\hat{H}[2r+1]P_p^u[2r+1]X_p[2r+1]\right|^2. \tag{1.50}$$

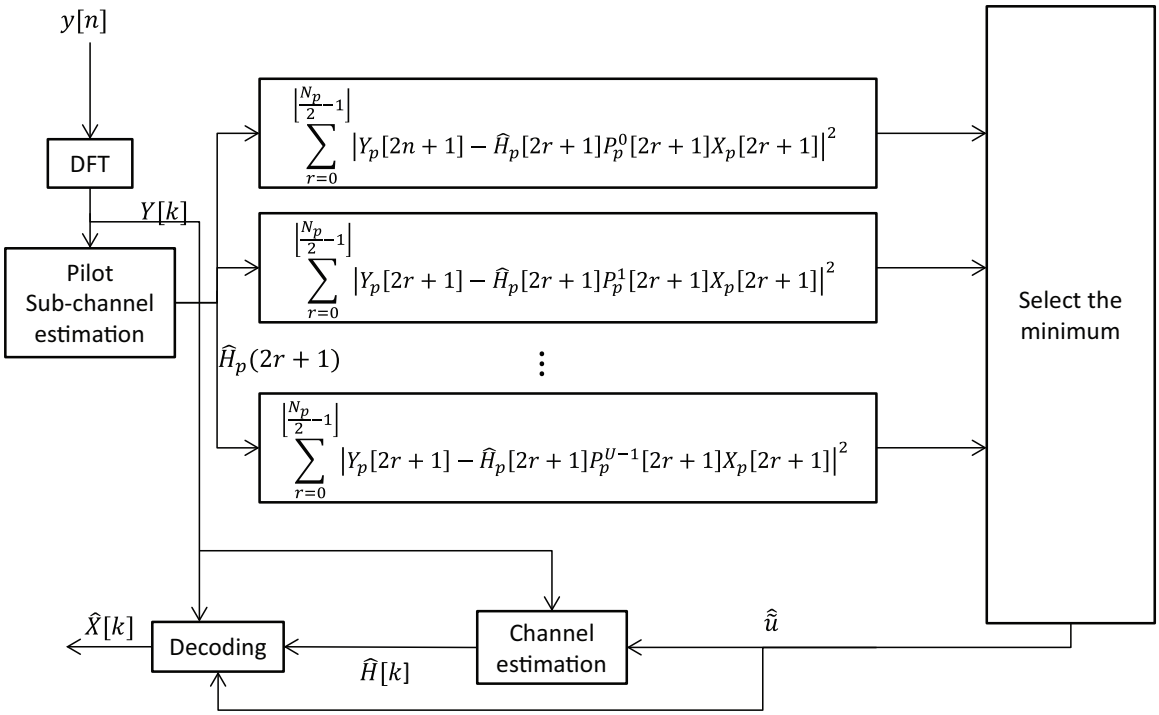

Figure 1.15: Pilot Sequence Detector.

The block diagram of the pilot sequences detection is shown in Fig 1.15. This scheme is based on a hybrid of ML and pilot-aided channel estimation. This scheme has low complexity than the conventional ML, however the modulation order influences the computational complexity, therefore it is unattractive to apply in higher order modulation.

1.5. Motivation of Research

The comparison of the PAPR reduction schemes is shown as Table 1.3. The simplest PAPR reduction scheme is clipping and filtering. Even though it does not require SI, it also does not lead the average power increment and bandwidth expansion while it causes BER performance degradation. TR scheme leads to increase the average power as well as bandwidth expansion and also requires large computational complexity although it does not cause BER performance degradation and SI requirement. SLM and PTS schemes are almost satisfied because they are distortionless. They do not involve the average power increasing and BER performance degradation. However, several IDFT operations at a transmitter demands large computational complexity and they require SI transmission that results in bandwidth expansion.

The SLM applied in the frequency domain changes the power or phase of complex input data. The FD-SLM generates phase factors to change the phase of the subcarries

Table 1.3: Comparison of PAPR reduction scheme [1–3].

Methods	Clipping	TR	PTS	SLM	TDC-SLM
Average Power Increase	No	Yes	No	No	No
Bandwidth Expansion	No	Yes	Yes	Yes	Yes
BER Degradation	Yes	No	No	No	No
Computational Complexity	Low	High	High	High	Low
Side Information	No	No	Yes	Yes	Yes

Table 1.4: Outline of the proposals.

Chapter 2	Purpose	Avoid to send SI in TDC-SLM.
	Research issue	In the existing TDC-SLM scheme requires sending SI to recover signal at receiver side that effect the throughput degradation.
	Proposed scheme	DC scheme is used to estimate cyclic shift in the TDC-SLM scheme.
	Achievement	The TDC-SLM with DC able to estimate the cyclic shift and has the BER performance closed to perfect estimation.
Chapter 3	Purpose	DC-MF for cyclic shift estimation scheme for multiple branches .
	Research issue	The trade-off PAPR reduction and BER in Chapter 2.
	Proposed scheme	Proposes a DC-MF scheme that improves the DC estimation scheme in Chapter 2.
	Achievement	The improvement of performance system even though it is applied in the linear PA.

in the frequency domain while the selection of the lowest PAPR is carried out in the time domain. Therefore, the FD-SLM requires many IDFT blocks and demands the high computational complexity. To overcome this computational complexity problem, a LC-SLM scheme has also been proposed and it utilizes two IDFT blocks [18,19,29,30,38–42]. The TDC-SLM reduces the computational complexity of the LC-SLM that uses only one IDFT. It reduces the PAPR more than the FD-SLM for the same number of phase rotation pattern candidates [43]. The BER performance can be preserved as the same as the FD-SLM, while SI transmission is still required. Thus, this thesis focuses on the TDC-SLM scheme. TDC-SLM is still required SI, several SI detection for FD-SLM and TD-SLM have been proposed as depicted in Fig. 1.16. Conversion matrix and sub-optimal SI detection schemes cause the throughput degradation, on the other hand the energy detection, pilot sequence, and maximum likelihood detection schemes have high computational complexity.

In this research, the TDC-SLM without SI transmission is proposed. The proposed

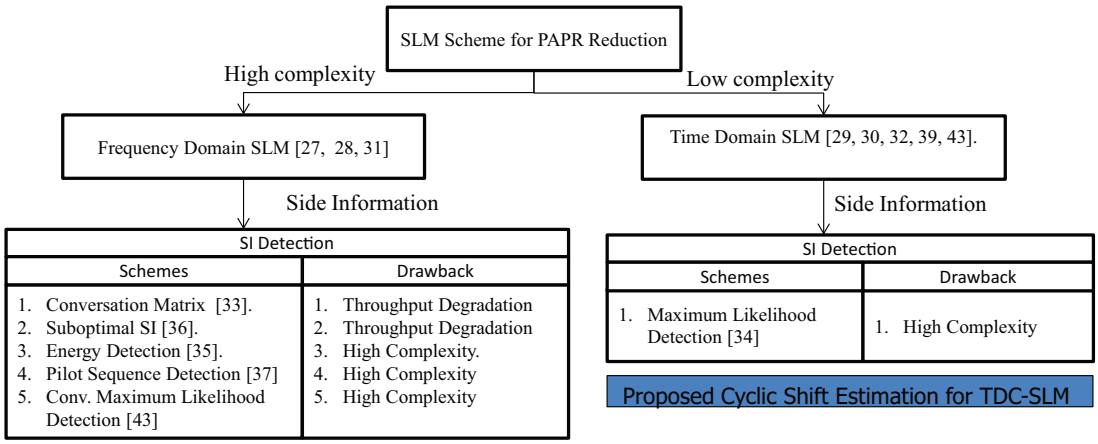

Figure 1.16: Historical of research.

scheme does not send SI. In the TDC-SLM, the transmitted signal constitutes of the original and its cyclically shifted signal. Therefore, the information of the amount of the cyclic shift is embedded in the transmitted signal. In other words, the information is not required to be send as SI separately. The information can be extracted in the receiver side by through cyclic shift estimation (DC or DC-MF). At a receiver side the amounts of the cyclic shifts are detected by using the delayed correlation (DC) for first research and delayed correlation and matched filter (DC-MF) for second research. In this proposed scheme, intervals between the cyclic shifts are designed so that the receiver can distinguish the cyclic shifts and multipath delays with the use of the DC and DC-MF. In the first research, even though PAPR is reduced however there is the trade-off between PAPR reduction and BER performance. Multiple branches for generating SCs is applied in the second research and it achieves better PAPR reduction than the previous research. Because the multipath components still deteriorate the accuracy rate of cyclic shift estimation since they generate additional peaks at the outputs of the cyclic shift estimation processing, in the second research the cyclic shift estimation processing is placed after the frequency domain equalization (FDE) to improve the accuracy of cyclic shift estimation. In this proposed research the PAPR reduction can be reduced and the received signal is recovered without sending SI. The BER performance of the proposed scheme is close to perfect estimation.

Chapter 1 consists the overview of OFDM and the PAPR problem, several PAPR reduction schemes that classified into frequency and time processing, SI detection schemes. The relationship of each chapter is shown in Fig. 1.17. The purpose, research issue, proposed scheme, and its achievement are summarized in Table 1.4. In Chapter 2 section 2.1, several SI detections are introduced in the SLM scheme. The DC scheme according to estimate cyclic shift for TDC-SLM is proposed in section 2.2.

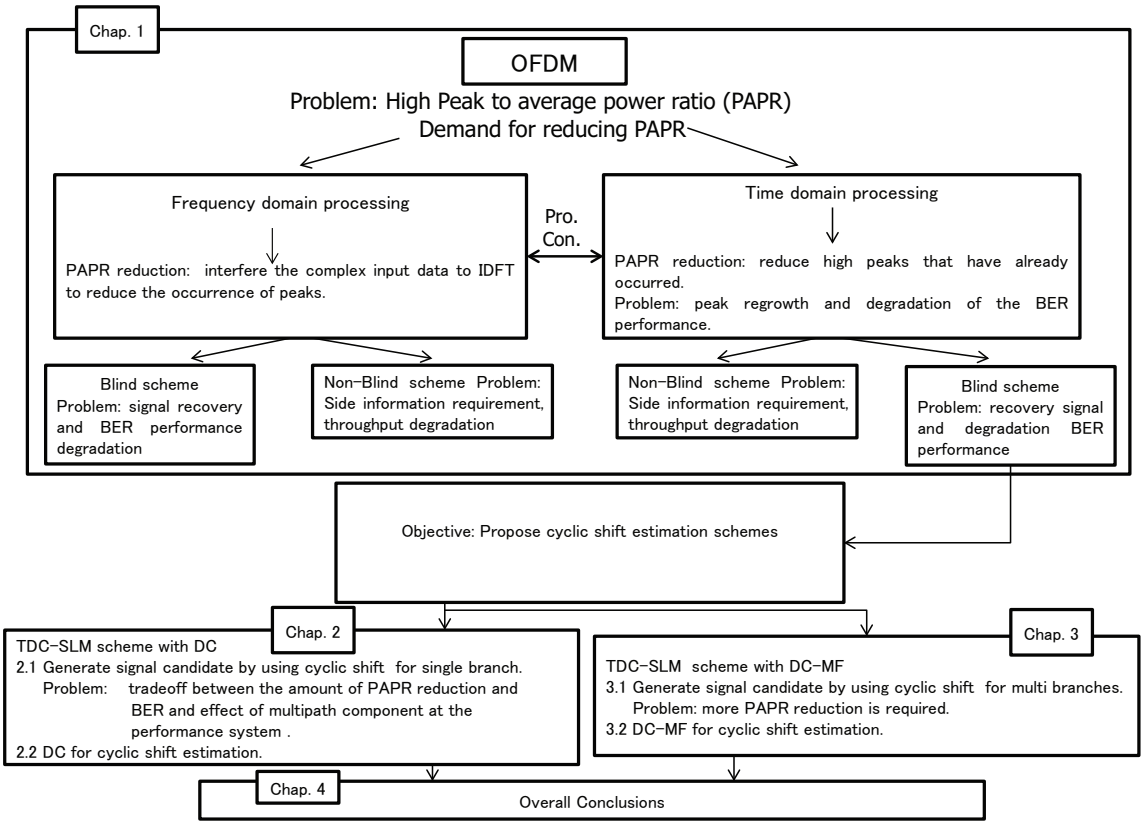

Figure 1.17: Overview Of thesis.

The proposed scheme able to estimate the cyclic shift for single branch in TDC-SLM scheme and the received signal can be recovered. In Chapter 3, the DC-MF scheme improves the DC scheme is proposed. In this scheme, the DC-MF is placed after frequency domain equalization (FDE) to remove multipath components in a received signal. It improves the system performance of the TDC-SLM without SI.

Chapter 2

Shift Estimation with Delayed Correlation Cyclic-Selective Mapping PAPR Reduction in OFDM System

2.1. Introduction

The TD-SLM reduces the computational complexity even though it still requires SI at the receiver to recover the original data which is usually transmitted as a set of bits (the SI bits). The error detection of the SI has an impact on the error performance that can be evaluated with a BER. In [29, 30], the SI is sent together with the transmitted signal and it causes the throughput degradation. The ML detection is used to estimate the SI in [32] which the computational complexity in the receiver side is affected by higher order modulation.

The DC estimation scheme that estimates cyclic shift in the TDC-SLM scheme is proposed in this Chapter. In the TDC-SLM scheme, the SCs generation are based on the TD-SLM scheme where the SC with the lowest PAPR is selected by summing the original signal in a time domain and its cyclically shifted version on single branch. The DC are utilized to estimate the amount of the cyclic shift based on the interval between the peaks at the output of the DC. The basic principal of the DC and DC-MF is to multiply the received signal by its conjugate guard interval which it is not affected by order modulation. Therefore, it is suitable to be implemented in many OFDM based application such as WLAN, ultra wideband (UWB) with an additional processing at the receiver side.

2.2. System Model

2.2.1. Time Domain Cyclic Selective Mapping

In the time domain, the OFDM signal $x[n]$ at the time index of n can be written as follows.

$$x[n] = \frac{1}{N} \sum_{k=0}^{N-1} X[k] \ \exp\left(j \frac{2\pi nk}{N}\right), \quad 0 \leqslant n \leqslant N-1, \tag{2.1}$$

where $X[k]$ is the data symbol on the k^{th} subcarrier, k is the subcarrier index, and N is the number of the subcarriers. The OFDM signal in the time domain is defined in a vector form as $\mathbf{x} = [x_0 \ x_1 \ .... \ x_{N-1}]^T$.

A GI is specified as a fraction of the OFDM symbol length and the GI sequence is appended to the beginning of the OFDM symbol as shown in Fig.1.6.

$$x_f[n] = \begin{cases} x[N+n], & n = -N_{GI}, -N_{GI}+1, ..., -1 \\ x[n], & n = 0, 1, ..., N-1. \end{cases} \tag{2.2}$$

The TDC-SLM process has been proposed to reduce the complexity of LC-SLM [30]. The TDC-SLM uses a time domain signal combining with cyclic delay and phase shift (TDSC-CP). It needs only one IDFT and overcomes the computional complexity issue while it achieves comparable PAPR reduction capability. The TDC-SLM uses the cyclic shift without scrambling of the original signal. The cyclically shifted signal of the TDC-SLM in the time domain are given as

$$x_c[n, \Delta] = \begin{cases} x[N-\Delta+n], & 0 \leqslant n \leqslant \Delta - 1 \\ x[n-\Delta], & \Delta \leqslant n \leqslant N-1, \end{cases} \tag{2.3}$$

where $x[n-\Delta]$ is the cyclically shifted signal and Δ is the amount of the cyclic shift which is a multiple of δ samples. δ is selected to be large enough in order to improve the accuracy of the cyclic shift estimation in the receiver. The SCs, $s_f[n]$, is generated by summation of the original signal and its cyclically shifted signal in the time domain as follows

$$s_f[n] = x_f[n] + x_f[n, \Delta], \tag{2.4}$$

where $s_f[n]$ with the lowest PAPR is chosen as the transmitted signal, $s[n]$, and $x_f[n, \Delta]$ denotes the cyclically shifted signal with the GI, which is given as

$$x_f[n, \Delta] = \begin{cases} x_c[n, \Delta], & 0 \leqslant n \leqslant N-1 \\ x_c[N+n, \Delta], & -N_{GI} \leqslant n < 0, \end{cases} \tag{2.5}$$

where $0 < \Delta < N - N_{GI}$. After summing the original signal and its cyclically shifted signal in Eq. (2.4), the SC that achieves the lowest PAPR is selected.

2.2.2. Delayed Correlation

The TDC-SLM needs the SI that decreases the throughput. Hence, the TDC-SLM without the SI is proposed. The DC will be applied to estimate the amount of the shift in the receiver side. In the TDC-SLM, the SC is obtained in Eq. (2.3) and the PAPR is calculated over the consecutive V OFDM symbols. The amount of the cyclic shift is then selected for the lowest average PAPR. Δ is recalculated in every V OFDM symbols. At the receiver, the received sample can be written as

$$y[n] = \sum_{i} h[i]s[n-i] + w[n], \tag{2.6}$$

where $h[i]$ represents the impulse response of a time-varying multipath channel, $w[n]$ is the zero-mean Gausian random vector with the covariance of σ^2 and it is independent of the input symbols. Here, it is assumed that coarse symbol synchronization is realized by preamble sequences transmitted prior to data symbols. The amount of the shift is detected through DC. Basically, this process multiplies the signal at the receiver in time domain with the conjugate of the GI sequence. When the last part of the OFDM symbol is multiplied with its conjugate that is appended as the GI, the highest peak output appears. It can be proven to Eq. (2.6) and the following Eq. (2.7) as

$$\begin{aligned}
c[n] &= y[n]y^*[n-N] \\
&= \left(\sum_{i} h[i]s[n-i] + w[n]\right) \\
&\times \left(\sum_{i'} h^*[i']s^*[n-N-i'] + w^*[n-N]\right) \\
&= \left(\sum_{i} h[i]s[n-i] \sum_{i'} h^*[i']s^*[n-N-i']\right) \\
&+ \left(\sum_{i} h[i]s[n-i]w^*[n-N]\right) \\
&+ \left(\sum_{i'} h^*[i']s^*[n-N-i']w[n]\right) \\
&+ w[n]w^*[n-N],
\end{aligned} \tag{2.7}$$

where $y[n]$ denotes the received symbol vector in the time domain, $y^*[n-N]$ is the

conjugate of the GI, $s[n-i] = s^*[n-N-i']$ and consequently

$$\begin{aligned} c[n] &= \sum_i |h[i]|^2 |s[n-i]|^2 \\ &+ \sum_i \sum_{i',i' \neq i} h[i]s[n-i]h^*[i']s^*[n-N-i'] \\ &+ \sum_i \left(h[i]s[n-i]\right) w^*[n-N] \\ &+ \sum_{i'} \left(h^*[i']s^*[n-N-i']w[n]\right) \\ &+ w[n]w^*[n-N]. \end{aligned} \tag{2.8}$$

The outputs of the multiplier are summed over the period of the GI, N_{GI}. After the summation, the outputs of the DC is averaged to the corresponding timing of the OFDM symbol as follows;

$$C[n] = \frac{1}{V} \sum_{v=1}^{V} \sum_{p=0}^{N_{GI}-1} c[n - v(N + N_{GI}) - p], \tag{2.9}$$

where V is the number of averaging symbols and p is the index for integration. The DC output requires to average symbols which needs the additional time to perform the averaging process. However, it is not significant. The first peak is found in the following maximization

$$\Delta_N^{\max} = \arg\max_n \left| C[n] \right|. \tag{2.10}$$

The DC is explained in Fig. 2.1 which generate outputs the correlation between the GI sequence and the received signal with the delay of $\hat{\Delta}$, i.e. $y[n-\hat{\Delta}]$. The GI consists of the last part of the original OFDM symbol sequence, $[x[N-N_{GI}]\ ...\ x[N]]$, as well as the last part of the SC sequence, $[x[N-N_{GI}-\Delta]\ ...\ x[N-1-\Delta]]$. Therefore, if $\hat{\Delta} = \Delta$, the DC also outputs another peak as explained in the following equations

$$\hat{c}_\Delta[n-\hat{\Delta}] = y[n-\hat{\Delta}]y^*[n-N], \tag{2.11}$$

where $y[n]$ denotes the received symbol vector in time domain, $y^*[n-N]$ is the conjugate of the GI, and $\hat{\Delta}$ is the amount of the delay. The Eq. (2.11) can be rewritten as

$$\hat{c}_\Delta[n-\hat{\Delta}] = \left(\sum_i h[i]s[n-\hat{\Delta}-i] + w[n-\hat{\Delta}] \right) \left(\sum_{i'} h^*[i']s^*[n-N-i'] + w^*[n-N] \right). \tag{2.12}$$

Substitute Eq. (2.6) into Eq. (2.7) yields

$$\begin{aligned} \hat{c}_\Delta[n-\hat{\Delta}] &= \left(\sum_i h[i]s[n-\hat{\Delta}-i] + \sum_i h[i]s[n-\hat{\Delta}-i,\hat{\Delta}] + w[n-\hat{\Delta}] \right) \\ &\times \left(\sum_i h^*[i']s^*[n-N-i'] + \sum_{i'} h^*[i']s^*[n-N-i'] + w^*[n-N] \right), \end{aligned} \tag{2.13}$$

and $s^*[n-i,\Delta] = s[n-\Delta-i]$ from the following relationship,

$$\begin{aligned}\hat{c}_\Delta[n,\hat{\Delta}] &= \left(\sum_i |h[i]|^2 |s[n-\hat{\Delta}]^2|\right) + \sum_i \sum_{i'} \Big(h[i]s[n-\hat{\Delta}-i]\Big) \\ &\times \quad (h[i']s^*[n-N-\Delta-i']) + w[n].w^*[n-N]. \end{aligned} \tag{2.14}$$

Thus, after the integration, the DC outputs the following,

$$\hat{C}_\Delta[n-\hat{\Delta}] = \frac{1}{V}\sum_{v=1}^{V}\sum_{p=0}^{N_{GI}-1} c[n-v(N+N_{GI})-\hat{\Delta}-p]. \tag{2.15}$$

The interval of the shift is set to one of every δ samples to improve the accuracy of the shift estimation at the receiver side. Since $\hat{\Delta}$ is not known at the receiver side, the second peak has to be found from

$$\Delta_{\text{2nd}}^{\max} = \underset{\hat{\Delta},\hat{\Delta}\neq N}{\arg\max} \left|\hat{C}_\Delta[n-\hat{\Delta}]\right|. \tag{2.16}$$

The amount of the shift $\hat{\Delta}_s$ is calculated from the interval of the peaks as

$$\hat{\Delta}_s = \Delta_N^{\max} - \Delta_{\text{2nd}}^{\max}. \tag{2.17}$$

2.2.3. Minimum Mean Square Error Detection

Preamble symbols are sent prior to data symbols to determine the frequency response of the channel as well as the symbol timing. The transmitted preamble symbol on the k^{th} subcarrier is represented as $S_{pre}[k]$ and the received preamble signal is given as

$$y_{pre}[n] = \sum_{i=0}^{N-1} h[i]s_{pre}[n-i] + w[n], \tag{2.18}$$

where $s_{pre}[n]$ and $y_{pre}[n]$ are the transmitted preamble signal and the received preamble signal at the time index of n. The received signal on the k^{th} subcarrier at the receiver is demodulated by taking the N -point normalized DFT as

$$Y_{pre}[k] = \sum_{n=0}^{N-1} y_{pre}[n]e^{-j2\pi nk/N}. \tag{2.19}$$

The channel estimation on the k^{th} subcarrier is given as follows.

$$\hat{H}[k] = Y_{pre}[k]/S_{pre}[k], \tag{2.20}$$

where $\hat{H}[k]$ is the estimated channel response on the k^{th} subcarrier. Because of the SLM in the time domain, the channel response needs to be modified during the data

period. The superposition of the data sequence works like an artificial multipath on the channel response. To calculate the channel response in the data period, the estimated channel response is converted to the impulse response in the delay domain as follows:

$$\hat{\mathbf{h}} = \text{IDFT}\left(\hat{\mathbf{H}}^{\text{H}}\right) = \left[\hat{h}[0] \;\; ... \;\; \hat{h}[N-1]\right]^{T}, \tag{2.21}$$

where $\hat{h} =$ is the i^{th} impulse response of the channel, $\hat{\mathbf{H}} = [\hat{H}[1] \; \hat{H}[2] \;\; ... \;\; \hat{H}[N]]$, and $\{.\}^{H}$ denotes the Hermitian transform. The impulse response will be shifted with the amount of $\hat{\Delta}_s$ in the delay domain and summed together with the original.

$$\hat{h}_{\Delta}[i] = \hat{h}[i] + \hat{h}[i - \hat{\Delta}_s]. \tag{2.22}$$

The channel response on the k^{th} subcarrier in the data period is

$$\hat{H}_{\Delta}[k] = \sum_{i=0}^{N-1} \hat{h}_{\Delta}[i] e^{-j2\pi ik/N}. \tag{2.23}$$

MMSE detection is used to avoid noise emphasis. The weight coefficient of the MMSE detection on the k^{th} subcarrier, $W_{\Delta}^{H}[k]$, is derived from

$$W[k] = \hat{H}_{\Delta}^{*}[k] \left(\hat{H}_{\Delta}[k]\hat{H}_{\Delta}^{*}[k] + \sigma^2\right)^{-1}. \tag{2.24}$$

The demodulated signal on the k^{th} subcarrier is given as

$$\hat{X}[k] = W[k]Y[k]. \tag{2.25}$$

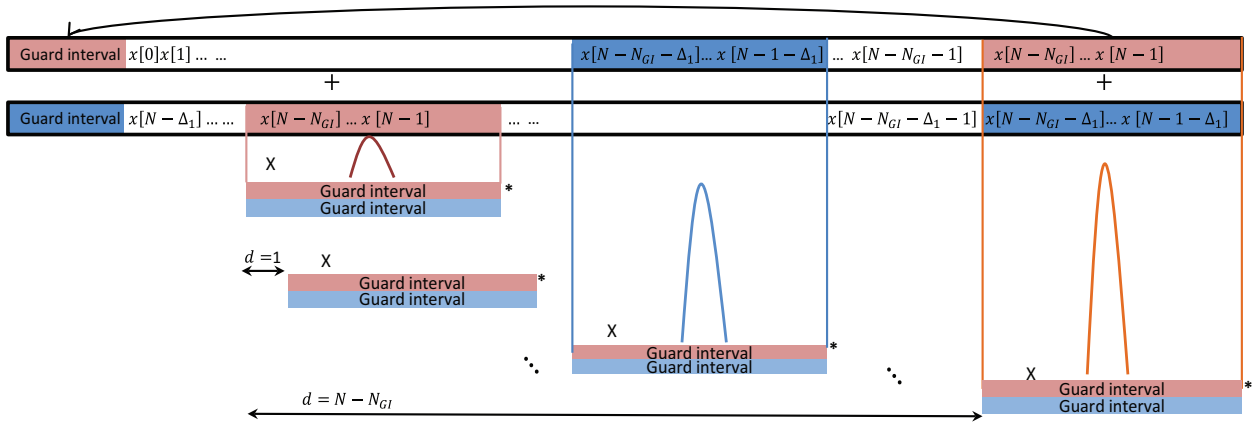

Figure 2.1: Delayed Correlation.

Table 2.1: Simulation Conditions.

Modulation	QPSK/OFDM
DFT Size	256
Number of Data Subcarriers	128
Eb/No	0,1,2,3...20
Guard Interval	0.25 DFT Size
Number of Symbols for Averaging	1,2,4,8 symbols
Interval of Cyclic Shift (Δ)	$\delta = 8$
Coding Scheme	Convolutional Coding
Interleaver	Matrix:16 $\times$ 8
Decoding Scheme	Soft Decision Viterbi Decoding
Constraint	7
Coding Rate	1/2
Channel	Uniform(6 path) GSM TU Exponential

2.3. Numerical Results

2.3.1. Simulation Conditions

The simulation is conducted in the specification conditions presented in Table 2.1 to measure the amount of PAPR reduction with the proposed scheme and to evaluate the BER of the system. The symbols are modulated into QPSK on each subcarrier where 10^4 data blocks are generated. The number of the subcarriers and the DFT size are 128 and 256, respectively. The length of the GI is 64 which is equal to a quarter of the DFT size. A convolutional code with the code rate of 1/2 and the constraint length of 7 is employed as channel coding. The matrix interleaver with the size of (16×8) is used. The number of the symbols for averaging L are 1, 2, 4, or 8. The interval of the shift is selected in every $\delta = 8$ samples. This simulation uses a GSM typical urban (GSM-TU) model, an exponential delay profile channel model, and a uniform delay profile channel model. The exponential delay profile has the maximum delay spread of 11 T_s with equally-spaced 12 paths and 1 dB decay per T_s while T_s is the sampling interval. The delay profile of the GSM-TU model is shown in Table 2.2. The uniform delay profile channel assumes 6 Rayleigh distribution paths with the uniform interval of T_s.

2.3.2. Complimentary Cumulative Distribution Function

Table 2.2: GSM Typical Urban Model.

Parth Number	1	2	3	4	5	6
Delay $\tau(\mu s)$	0	0.2	0.5	1.6	2.3	5
Power $P[\pi](dB)$	-3	0	-2	-6	-8	-10

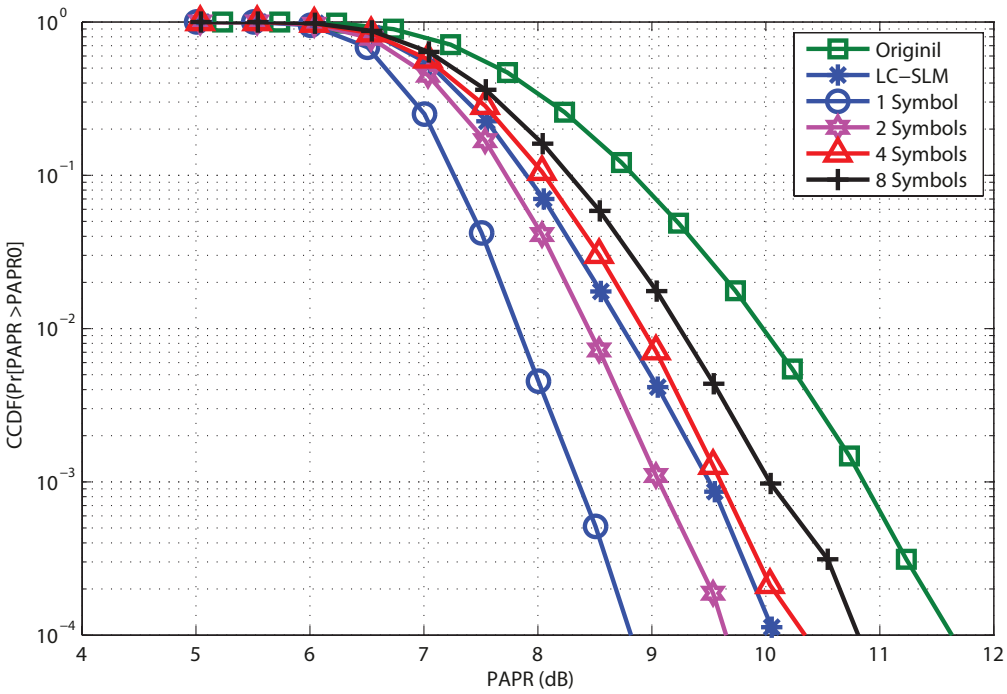

Figure 2.2: PAPR Reduction with SLM, LC-SLM, and Cyclic SLM.

The PAPR performance curves of the original, the LC-SLM and the TDC-SLM have been evaluated through computer simulation in Fig. 2.2. The CCDF of PAPR for the original signal and the TDC-SLM, the proposed scheme provides significant PAPR reduction. It appears that the curve with $L = 1$ symbol for averaging has the highest PAPR reduction which is about 2.9 dB lower than the original signal at the CCDF of 10^{-4}. The reduction takes place because every 1 OFDM symbol has a different cyclic shift δ in the consequence, therefore it preponderant to obtain the lowest PAPR than 2, 4, or 8 symbol for averaging. Using 2, 4, and 8 symbol for averaging will only reduce 2.1 dB, 1.7 dB and 0.9 dB at the CCDF of 10^{-4} as compared to the original signal. On the other hand, if the number of symbols for averaging is 4, the amount of PAPR reduction is quite close to the LC-SLM. Nevertheless, the cyclic SLM has a low computational complexity considering that it only uses 1 IDFT.

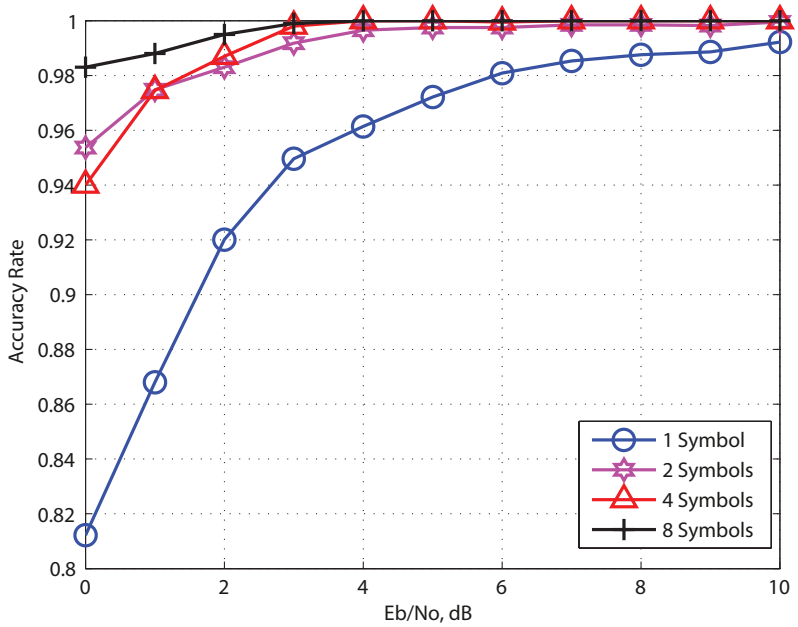

Figure 2.3: Accuracy Rate on Uniform Delay Profile Channel.

2.3.3. Accuracy Rate

The interval of cyclic shift is 8 which is selected to be large in order to improve the accuracy of the cyclic shift estimation at the receiver side. If the interval is quite small when the noise is increased, the circular shift estimation will be shifted and incorrect. Figures 2.3, 2.4, and 2.5 show the accuracy rate in the estimation of the amount of the cyclic shift at the receiver side. A uniform delay profile, the GSM TU and an exponential channel are assumed. It appears that the third channel have the accuracy rate around of 98% and 99% over 1 or 2 symbols for averaging. Whereas, averaging over 4 or 8 symbols achieves an accuracy rate close to 100 % at $E_b/N_0 = 8$ dB and $E_b/N_0 = 7$ dB.

2.3.4. Bit Error Rate

The BER performance will be evaluated on different channel conditions. For BER evaluation convolutional coding with the polynomial of [171 133] and matrix interleaving are applied. The BER with ideal power amplifier (PA) and no PAPR reduction is included as a reference. Figures 2.6, 2.7, and 2.8 show the comparisons of the BER curves with 1, 2, 4, and 8 symbols for averaging on each channel. From these figures, it is clear that the averaging over 1 or 2 symbols shows higher BERs than those with 4 and 8 symbols under the same E_b/N_0 conditions, while the curves with the averaging of 4 and 8 symbols have only little difference and those curves show slightly different

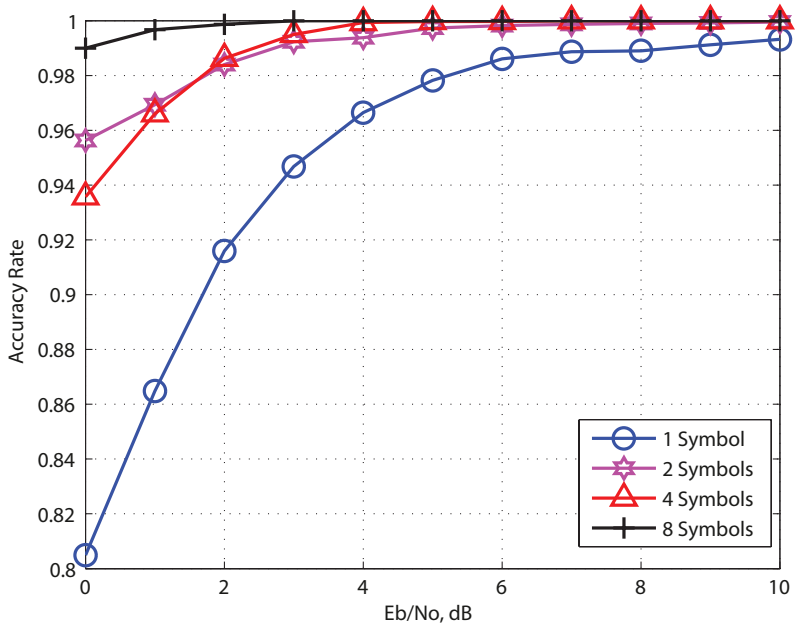

Figure 2.4: Accuracy Rate on Exponential Delay Profile Channel.

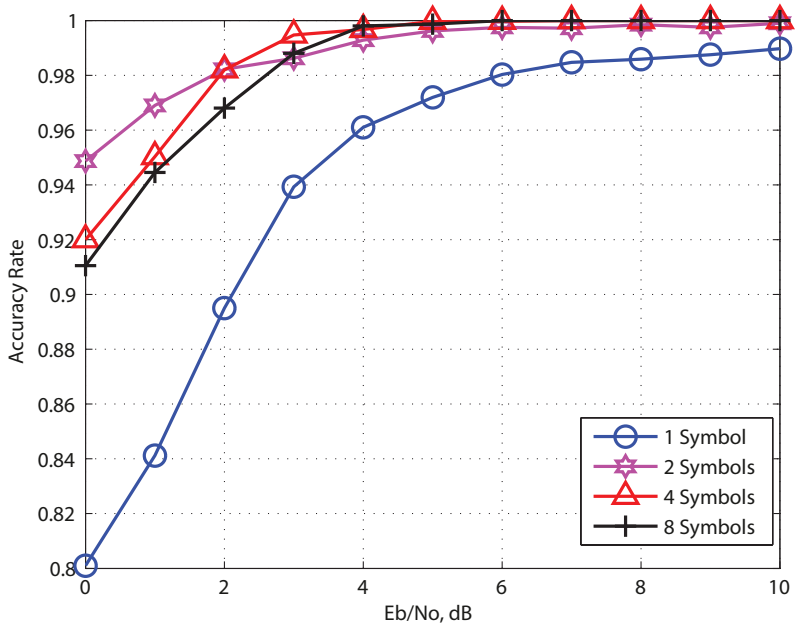

Figure 2.5: Accuracy Rate on GSM TU Channel.

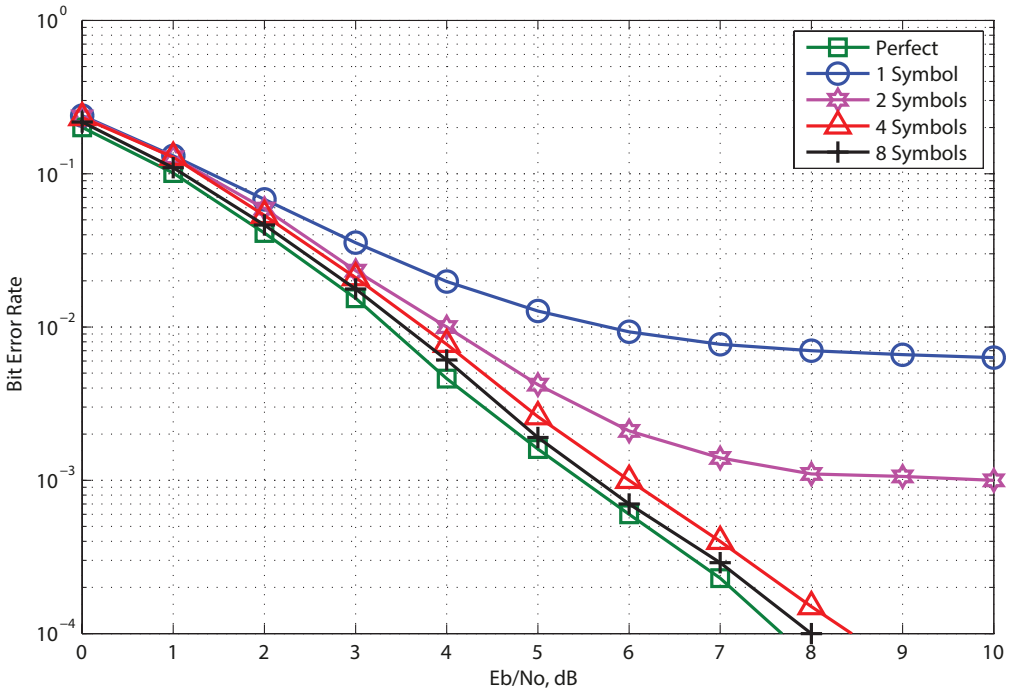

Figure 2.6: BER on Uniform Delay Profile Channel.

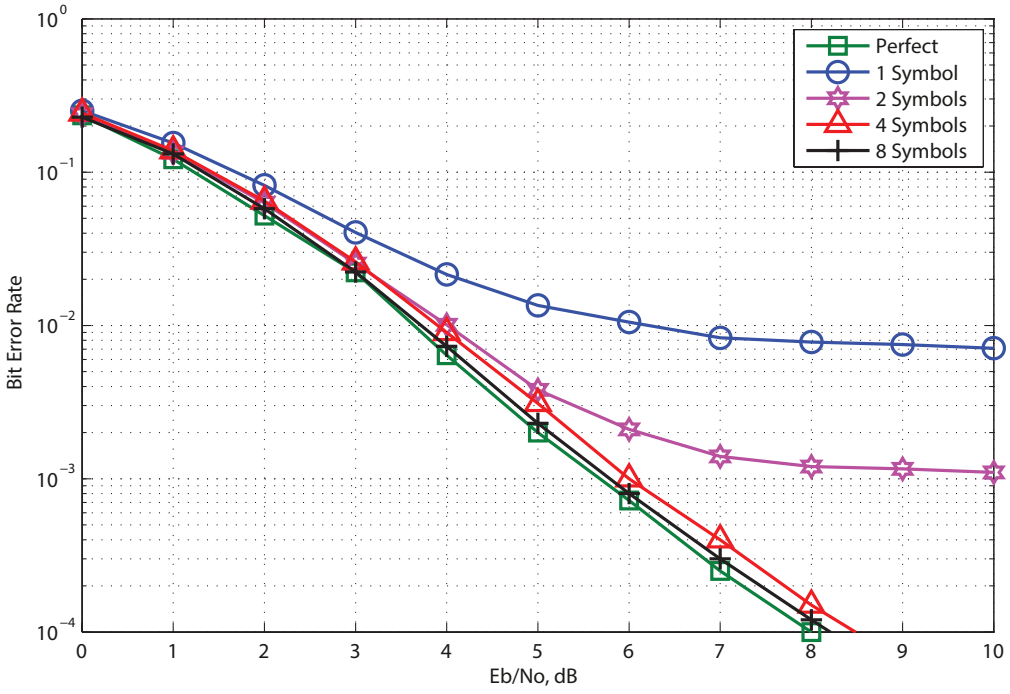

Figure 2.7: BER on Exponential Delay Profile Channel.

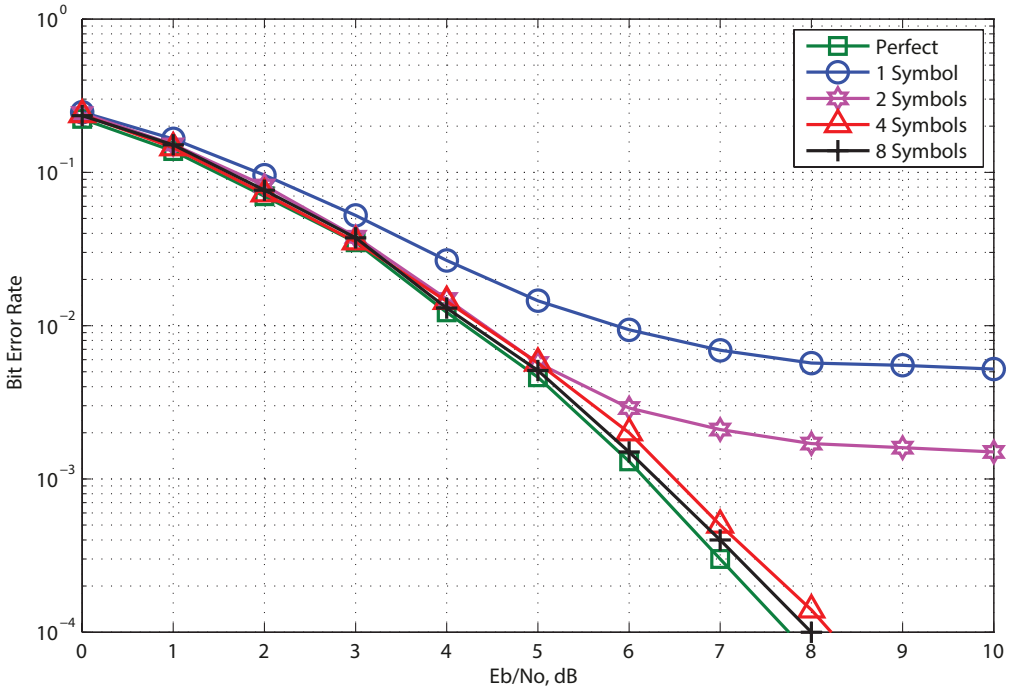

Figure 2.8: BER on GSM TU Channel.

degradation from that with perfect shift estimation. This is because of the accuracy rate difference of the cyclic shift estimation.

2.4. Conclusions

The TDC-SLM scheme with no SI has been presented in this chapter. The TDC-SLM is applied to reduce the PAPR with the low complexity implementation that uses only one IDFT while DC is used to estimate the amount of the shift at the receiver. Numerical results obtained through computer simulation show that there is a trade-off between the amount of PAPR reduction and the BER. If the number of symbols for averaging to estimate the amount of the cyclic shift is 4 symbols, the amount of PAPR reduction is quite close to that at the LC-SLM scheme while the accuracy of the cyclic shift estimation is more than 0.99 at $E_b/N_0 = 8$ dB.

Chapter 3

Estimation of Cyclic Shift with Delayed Correlation and Matched Filtering in Time Domain Cyclic Selective Mapping

3.1. Introduction

In Chapter 2, the TDC-SLM with DC is applied to reduce a PAPR and to estimates the amount of a cyclic shift at the receiver without SI transmission [44]. The time domain SCs generate with single branch at the transmitter side then the SC with the lowest PAPR is chosen for transmission. The cyclic shift estimation by using the DC is affected with the channel condition. When the noise increases, the cyclic shift estimation will be shifted. Therefore, the same amount of the cyclic shift are required for several OFDM symbols in order to improve the accuracy rate of the cyclic shift estimation. Nevertheless, there is a trade-off between the amount of PAPR reduction and the BER.

The DC-MF is proposed to overcome the trade-off between PAPR reduction and BER performance. In Chapter 2, the greater PAPR reduction is occurred when 1 symbol for averaging is applied otherwise it causes BER performance degradation. The SCs are generated by multiple branches at the transmitter side. The original signal is summed with its shifted version where the shifted signal has different cyclic shift for every branch. The multiple branches do not cause ISI because the summation of the original and its cyclically shifted signal is processed before adding guard interval. The summation process is performed for every OFDM symbol if the length of GI is enough to overcome the multipath fading then it will not cause ISI. A Barker code sequences

is used to decrease the amount of combination for cyclic shift.

The DC-MF process consists of DC and MF which is implemented to estimate the cyclic shift for the use multiple branches. The MF ables to detect the consecutive peak from the DC output as the amounts of the cyclic shifts estimation at the receiver. The DC-MF places after FDE to remove multipath components in a received signal. At a transmitter side, a transmit signal is generated by the summation of an original signal and signals with cyclic shifts. At a receiver side the amounts of the cyclic shifts are detected by using the DC-MF.

In this proposed scheme, intervals between the cyclic shifts are designed so that the receiver can distinguish the cyclic shifts and multipath delays with the use of the MF. However, multipath components still deteriorate the accuracy rate of cyclic shift estimation since they generate additional peaks at the outputs of the DC-MF. By using the proposed scheme, the accuracy rate then improves and the BER reduces as compared to that of the conventional TDC-SLM and DC-MF in [45].

3.2. System Model

3.2.1. Multiple Branches in TDC-SLM

The discrete OFDM signal $x[n]$ in time domain can be written as:

$$x[n] = \frac{1}{N} \sum_{k=0}^{N-1} X[k] \ \exp\left(j \frac{2\pi nk}{N}\right), \ 0 \leqslant n \leqslant N-1, \tag{3.1}$$

where n is the time index, $X[k]$ is the data symbol on the k^{th} subcarrier, k denotes the subcarrier index, and N is the number of the subcarriers. The OFDM signal can also be defined as a vector $\mathbf{x} = [x[0] \ x[1] \ .... \ x[N-1]]^T$.

In order to mitigate the intersymbol interference, a GI is needed. The GI can be obtained by copying the last part of the OFDM signal and adding it to the beginning of the signal.

$$x_f[n] = \begin{cases} x[n], & 0 \leqslant n \leqslant N-1 \\ x[N+n], & -N_{GI} \leqslant n < 0, \end{cases} \tag{3.2}$$

where N_{GI} is the length of the GI.

In the TDC-SLM scheme, a signal on each branch is generated by applying a cyclic shift to the original signal. The block diagram of the TDC-SLM scheme is shown in Fig. 3.1. The cyclically shifted signal in the TDC-SLM is given as

$$x_f[n, \Delta_d] = \begin{cases} x[N-\Delta_d+n], & -N_{GI} \leqslant n \leqslant \Delta_d - 1 \\ x[n-\Delta_d], & \Delta_d \leqslant n \leqslant N-1, \end{cases} \tag{3.3}$$

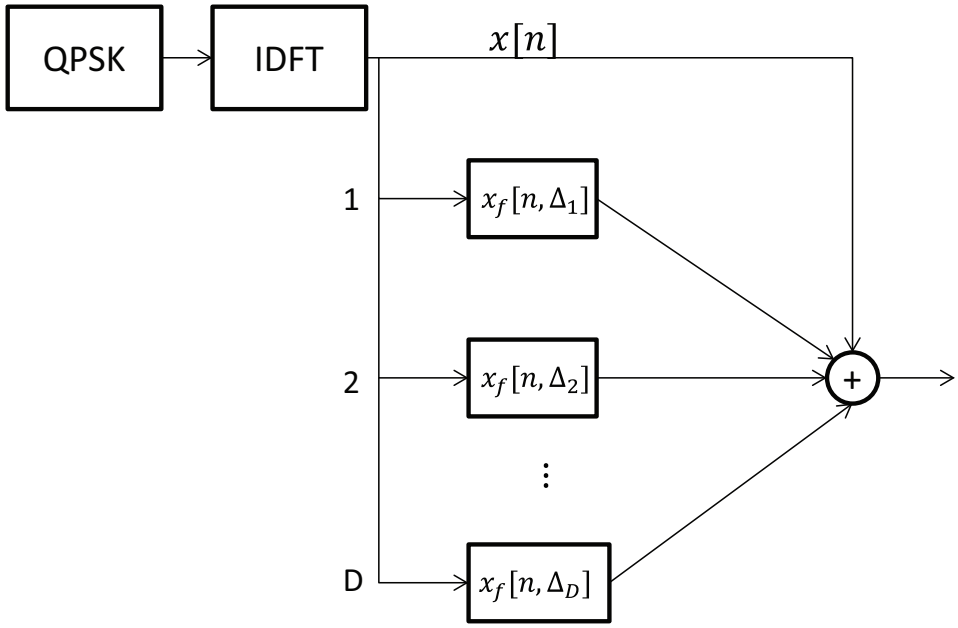

Figure 3.1: TDC-SLM with ($D = 3$) signal candidates.

where $x[n]$ is the OFDM signal in the time domain at the time index of n, N_{GI} is the GI length, $x_f[n, \Delta_d]$ is its cyclically shifted signal by Δ_d, Δ_d is the amount of the cyclic shift for the d^{th} cyclically shifted signal , and $\Delta_d \in \{C\delta\}$ where C is an integer [44, 45]. The resolution of the cyclic shifts, δ, has to be large enough for accurate estimation of the cyclic shifts in a receiver.

The SCs, $s_f[n]$, is the summation of the the original signal and its cyclically shifted signal in the time domain as follows:

$$s_f[n] = x_f[n] + \sum_{d=1}^{D} Q_d x_f[n, \Delta_d], \tag{3.4}$$

where $s_f[n]$ with the lowest PAPR is chosen as the transmit signal, $s[n]$, D is the number of branches, Q_d is the d^{th} coefficient in the phase sequence, and $x_f[n]$ is the original signal with the GI. The same set of $\{\Delta_d\}$ is applied over multiple symbols since the corresponding outputs of the DC-MF are averaged to improve the accuracy of cyclic shift estimation. Thus, the set of $\{\Delta_d\}$ is selected so that the maximum PAPR over the symbols for averaging is minimized. Here, the PAPR is calculated for each OFDM symbol period.

$$\text{PAPR}(s_f[n]) = \underset{0 \leqslant n \leqslant N-1}{10\log_{10}} \left[\frac{\max |s_f[n]|^2}{\text{E}\{|s_f[n]|^2\}} \right], \tag{3.5}$$

where E{.} denotes the expectation operation.

3.2.2. Channel Estimation and Frequency Domain Equalization

Frequency response and coarse symbol timing can be obtained by sending the preamble symbols at the beginning of the transmitted signal. The received preamble signal is given by

$$y_{pre}[n] = \sum_{i=0}^{N-1} h[i]s_{pre}[n-i] + w[n], \tag{3.6}$$

where $s_{pre}[n]$ and $y_{pre}[n]$ are the n^{th} transmitted and received preamble signals in the time domain, respectively. At the receiver, the preamble signal on the k^{th} subcarrier is demodulated by taking a discrete Fourier transform (DFT) as

$$Y_{pre}[k] = \sum_{n=0}^{N-1} y_{pre}[n]e^{-j2\pi nk/N}. \tag{3.7}$$

The estimation of the channel frequency response on the k^{th} subcarrier in the frequency domain, $\hat{H}[k]$, is given as follows:

$$\hat{H}[k] = Y_{pre}[k]/S_{pre}[k], \tag{3.8}$$

where $S_{pre}[k]$ is the transmitted preamble symbols on the k^{th} subcarrier. Because of the TDC-SLM in the time domain, the channel frequency response needs to be modified during the data period. The superposition of the data sequence works like an artificial multipath on the channel response. To calculate the channel frequency response in the data period, the estimated channel response is converted to the impulse response in the delay domain as follows:

$$\hat{\mathbf{h}} = \text{IDFT}\left(\hat{\mathbf{H}}^{\text{T}}\right) = \left[\hat{h}[0] \;\; ... \;\; \hat{h}[N-1]\right]^T, \tag{3.9}$$

where $\hat{h}[i]$ is the i^{th} impulse response of the channel, $\hat{\mathbf{H}} = [\hat{H}[1] \; \hat{H}[2] \;\; ... \;\; \hat{H}[N]]^T$, and $\{.\}^T$ denotes the transpose.

The coefficients of the minimum mean square error (MMSE)-frequency domain equalization (FDE) for the k^{th} subcarrier, $W[k]$, is given by

$$W[k] = \hat{H}^*[k]\left(\hat{H}[k]\hat{H}^*[k] + \sigma^2\right)^{-1}, \tag{3.10}$$

where $\hat{H}^*[k]$ denotes the conjugate of the channel frequency response that is obtained from Eq. (3.8) and σ^2 is the variance of the noise estimated in the receiver. The demodulated signal on the k^{th} subcarrier is then

$$\hat{Y_r}[k] = W[k]Y[k], \tag{3.11}$$

where $Y_r[k]$ denotes the signal on the k^{th} subcarrier at the receiver.

3.2.3. Delayed Correlation and Matched Filter Scheme

The DC-MF is applied to the signal in the time domain after the MMSE-FDE to estimate the amounts of the cyclic shifts at the receiver. The received signal in the time domain can be written as

$$\begin{aligned} y_r[n] &= \frac{1}{N}s[n]\sum_{k=1}^{N}\frac{F_{n,k}^{*}F_{n,k}|H[k]|^2}{|H[k]|^2+N_0/E_s}+\frac{1}{N}\sum_{\substack{l\neq n\\ l=1}}^{N}\sum_{k=1}^{N}S[k]\frac{F_{l,k}^{*}|H[k]|^2}{|H[k]|^2+N_0/E_s} \\ &+ \sum_{k=1}^{N}W[k]\frac{F_{n,k}^{*}|H[k]|^2}{|H[k]|^2+N_0/E_s}, \end{aligned} \tag{3.12}$$

where $H[k]$ is the channel frequency response, $S[k]$ is the signal component, and $W[k]$ is the Gaussian noise on the k^{th} subcarrier. Furthermore, $y_r[n]$ is the n^{th} received signal, E_s/N_0 is the signal-to-noise ratio per sample, $F_{n,k}=\exp\left[j\frac{2\pi nk}{N}\right]/\sqrt{N}$, N is the size of the DFT, and $\{.\}^*$ denotes conjugate. The DC-MF process consists of DC and MF as shown in Fig. 3.2. In the transmitter side, the TDC-SLM generates several SCs by summing the original signal with its cyclically shifted signals after the IDFT and generates the transmit signal through the summation of the original signal and the its cyclically shifted signals. The DC-MF is utilized to estimate the amount of the cyclic shifts since they are required to recover the transmit signal.

Basically, the DC process multiplies the received signal in the time domain with the conjugate of the GI sequence. The largest peak appears when the last part of the OFDM symbol is multiplied with the conjugate of the GI. The output of the DC is put into the MF to estimate the set of the cyclic shifts, $\{\Delta_d\}$, by detecting the second largest peak output. The DC-MF processes with 3 branches are shown in Fig. 3.3. The DC is defined as follows:

$$\begin{aligned} c[n] &= y_r[n]y_r^{*}[n-N] \\ &= \Big(\frac{1}{N}s[n]\sum_{k=1}^{N}\frac{F_{n,k}^{*}F_{n,k}|H[k]|^2}{|H[k]|^2+N_0/E_s}+\frac{1}{N}\sum_{\substack{l\neq n\\ l=1}}^{N}\sum_{k=1}^{N}S[k]\frac{F_{l,k}^{*}|H[k]|^2}{|H[k]|^2+N_0/E_s} \\ &+ \sum_{k=1}^{N}W[k]\frac{F_{n,k}^{*}|H[k]|^2}{|H[k]|^2+N_0/E_s}\Big)\times\Big(\frac{1}{N}s^{*}[n-N]\sum_{k=1}^{N}\frac{F_{n,k}^{*}F_{n,k}|H[k]|^2}{|H[k]|^2+N_0/E_s} \\ &+ \frac{1}{N}\sum_{\substack{l\neq n\\ l=1}}^{N}\sum_{k=1}^{N}S^{'}[k]\frac{F_{l,k}^{*}|H[k]|^2}{|H[k]|^2+N_0/E_s}+\sum_{k=1}^{N}W^{'}[k]\frac{F_{n,k}^{*}|H[k]|^2}{|H[k]|^2+N_0/E_s}\Big), \end{aligned} \tag{3.13}$$

where $s[n]=s^{*}[n-N]$, $S^{'}[k]$ and $W^{'}[k]$ are the signal and noise components on the k^{th}

subcarrier output from the delayed branch of the DC, respectively. After the summation, the outputs of the DC are averaged as follows:

$$C[n] = \frac{1}{V}\sum_{v=1}^{V}\sum_{p=0}^{N_{GI}-1} c[n - v(N + N_{GI}) - p], \tag{3.14}$$

where V is the number of symbols used in the averaging process. The first peak is caused by the GI and is found by maximization as

$$n^{\max} = \arg\max_{n} |C[n]| . \tag{3.15}$$

In addition, the DC produces the correlation between the GI sequence and the received signal with the delay of $\hat{\Delta}_d$, i.e., $y_r[n - \hat{\Delta}_d]$. The transmitted signal in the GI consists of the last part of the original OFDM signal, $[x[N - N_{GI}] \; ... \; x[N]]$, as well as the last part of the SC sequence, $[x[N - N_{GI} - \Delta_d] \; ... \; x[N - 1 - \Delta_d]]$. Hence, if $\hat{\Delta}_d = \Delta_d$, the DC outputs another peak as follows:

$$\hat{c}_d[n^{\max} - \hat{\Delta}_d] = y_r[n^{\max} - \hat{\Delta}_d] y_r^*[n^{\max} - N], \tag{3.16}$$

where $\hat{\Delta}_d$ is the candidate for the amount of the cyclic shift on the d^{th} branch. Eq. (3.16) can be rewritten as

$$\begin{aligned}\hat{c}_d[n^{\max} - \hat{\Delta}_d] = &\left(\sum_i h[i] s[n^{\max} - \hat{\Delta}_d - i] + w[n^{\max} - \hat{\Delta}_d]\right) \\ &\times \left(\sum_{i'} h^*[i'] s^*[n^{\max} - N - i'] + w^*[n^{\max} - N]\right).\end{aligned} \tag{3.17}$$

Therefore, the d^{th} peak output of the DC is given as

$$\hat{C}_d[n^{\max}, \hat{\Delta}_d] = \frac{1}{V}\sum_{v=1}^{V}\sum_{p=0}^{N_{GI}-1} \hat{c}_d[n^{\max} - v(N + N_{GI}) - \hat{\Delta}_d - p]. \tag{3.18}$$

The outputs of the DC are then passed to the MF to estimate the amounts of the cyclic shifts. Figure 3.4 shows the structure of the MF. In order to reduce the number of the combinations of $\{\Delta_d\}$, here, the amounts of the cyclic shifts are selected from every δ samples as $\{\Delta, \Delta + \delta, ..., \Delta + (d-1)\delta\}$. The structure of the MF has the delay line in which all the delays are set to $(\delta - 1)$. The output of the MF is expressed as follows:

$$\hat{C}_m[n^{\max}, \hat{\Delta}] = \sum_{d=1}^{D} Q_d \hat{C}_d[n^{\max}, \hat{\Delta} + (\delta - 1)(d - 1)], \tag{3.19}$$

where $\hat{C}_m[n^{\max}, \hat{\Delta}]$ is the output of the MF, Q_d is the d^{th} coefficient in the phase sequences (Barker sequence).

The cyclic shift of the first branch, Δ, is estimated through maximization as

$$\Delta^{\max} = \arg\max_{\hat{\Delta}} \left| \hat{C}_m[n^{\max}, \hat{\Delta}] \right|, \tag{3.20}$$

where $\Delta^{\max}$ is the estimated amount of the cyclic shift for the first branch, Δ. The channel impulse response in Eq. (3.9) is shifted by the estimated cyclic shifts and summed together with the original impulse response as follows:

$$\hat{h}_d[i] \;=\; \sum_{d=1}^{D} \left(\hat{h}[i] + \hat{h}[i - (\Delta^{\max} + (\delta - 1)(d - 1)] \right). \tag{3.21}$$

The received signal in the frequency domain after channel compensation is given as follows:

$$\hat{X}[k] = \hat{H}_d[k] Y[k], \tag{3.22}$$

where the channel response on the k^{th} subcarrier in the data period is

$$\hat{H}_d[k] = \sum_{i=0}^{N-1} \hat{h}_d[i] \exp\left(-j2\pi ik/N\right). \tag{3.23}$$

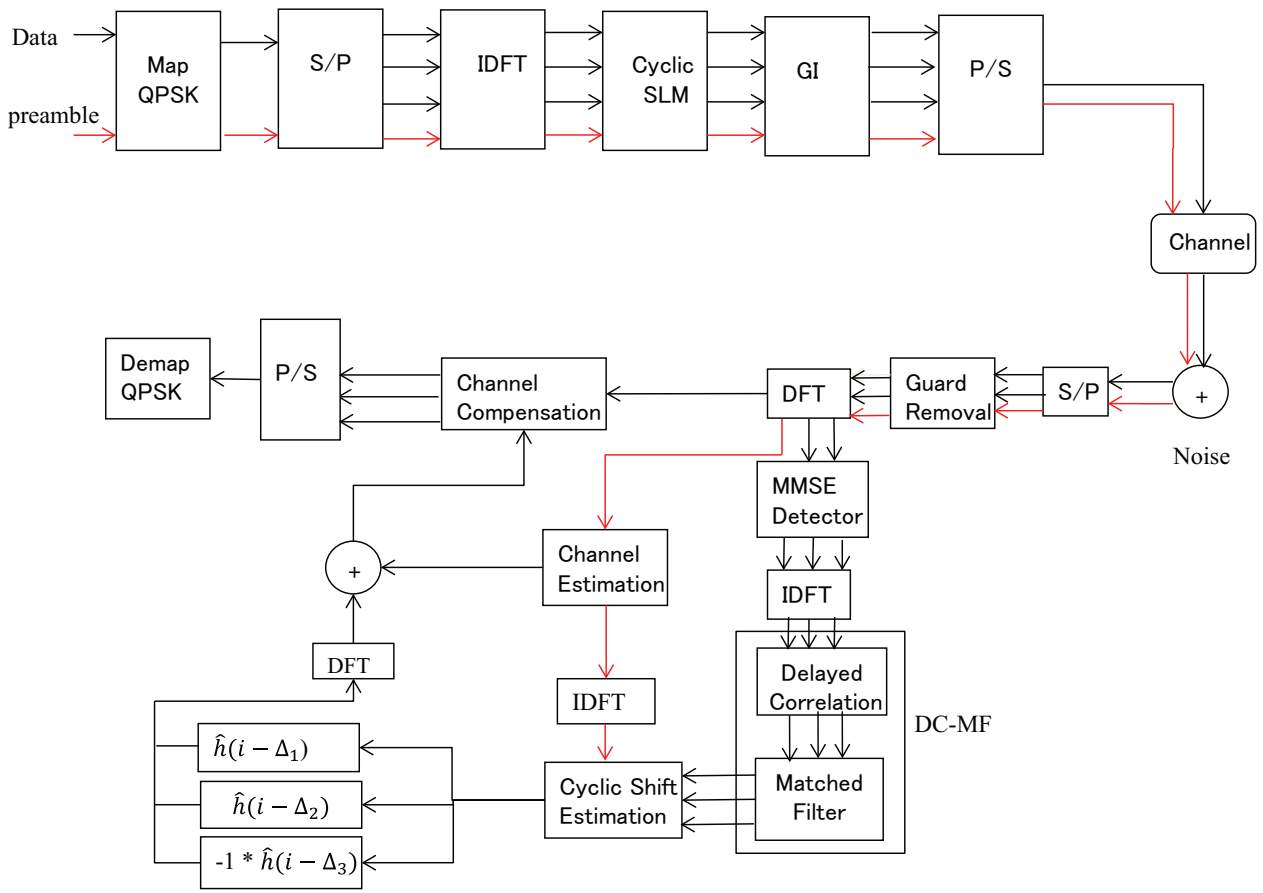

Figure 3.2: Block diagram of proposed scheme.

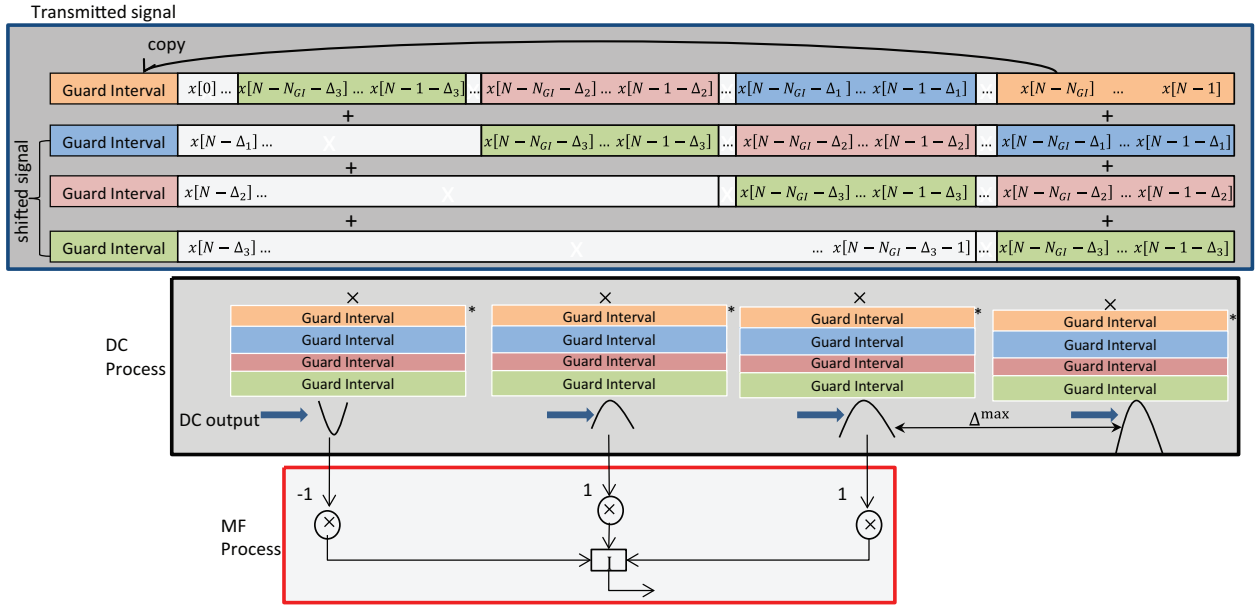

Figure 3.3: Delayed correlation ($D = 3$).

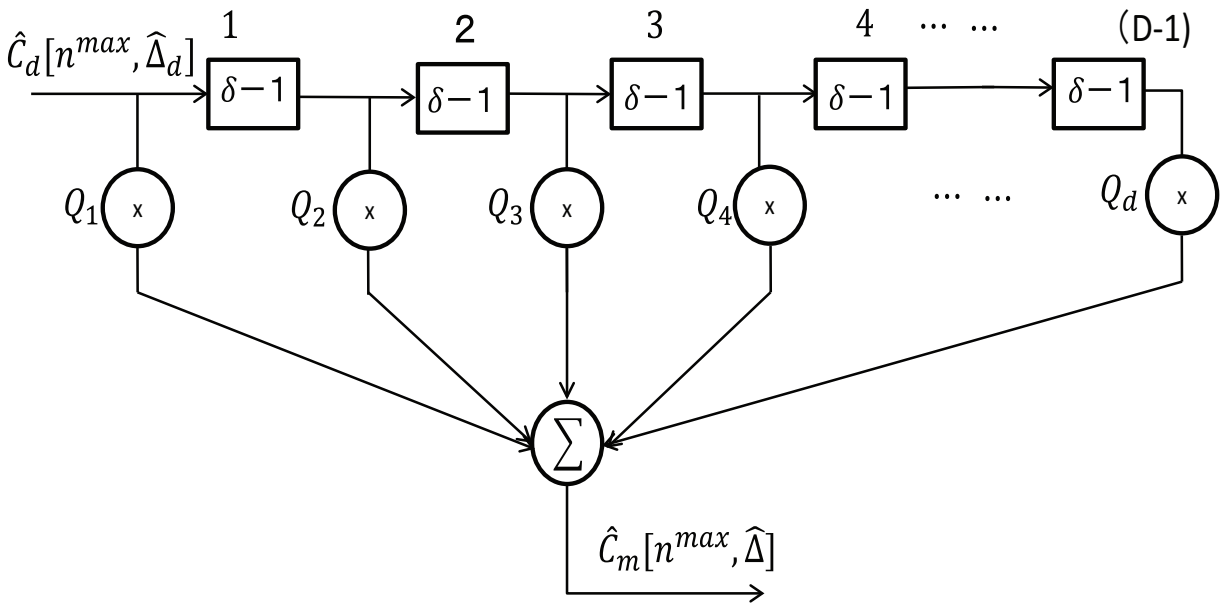

Figure 3.4: Matched filter.

3.3. Numerical Results

3.3.1. Simulation Conditions

Table 3.1 shows the simulation parameters of the proposed scheme which are adopted from LTE parameters. The number of data subcarriers is 128 and each subcarrier is modulated with QPSK. The DFT size is 256 and the length of the GI is set to be 64 samples. The number of symbols for averaging is set to 1, 2, 4, or 8, and the range of the cyclic shift (Δ_d) is limited from 60 to 124 with the resolution of every 4 samples (δ), which means 16 SCs. A convolutional code with a rate of 1/2 and constraint length of 7 with polynomial generator [171 133] is applied. The block interleaver with a size of 16×8 is applied. The number of branches is 3 and a Barker sequence with a length of 3 (Q_d) is used as the phase sequence. A uniform delay profile with 6 paths is assumed as the channel model in computer simulation. As a nonlinier HPA Rapp's solid state power amplifier model (SSPA) with a knee factor of 3 is assumed. The input back off (IBO) for the HPA is set to 0, 2, and 4 dB.

3.3.2. PAPR Reduction

3.3.3. PAPR Reduction

The PAPR performance curves are evaluated in term of complementary cumulative

Table 3.1: Simulation Conditions.

Modulation	QPSK/OFDM
DFT Size	256
Number of Data Subcarriers	128
Guard Interval	64
Number of Symbols for Averaging	1,2,4,8 Symbols
Cyclic Shift (Δ_d)	from 60 until 124
Resolution of Cyclic Shift (δ)	4
Coding Scheme	Convolutional Coding
Interleaver	Matrix:16× 8
Decoding Scheme	Soft Decision Viterbi
Constraint Length	7
Coding Rate	1/2
Polynomial Generator	[171 133]
Number of Branches	3
Channel	Uniform (6 paths)
Knee Factor Power Amplifier (p)	3
Input Back Off (IBO)	0, 2, 4 dB

distribution functions (CCDF). The TDC-SLM assumes $D = 3$ branches with the cyclic shift resolution of $\delta = 4$ and the number of the symbols for averaging is selected from 1, 2, 4, or 8. From Fig. 3.5, it can be seen that in comparison with the original signal, the amounts of PAPR reduction in the TDC-SLM for 1, 2, 4, or 8 symbols for averaging are 2.8 dB, 2.7 dB, 2.6 dB, and 2.5 dB, respectively, at the CCDF of 10^{-4}. When the number of symbols for averaging is 1, each OFDM symbol has different set of the cyclic shifts and the best PAPR reduction is achieved. On the other hand, the smallest amount of PAPR reduction is realized where 8 OFDM symbols have the same set of the cyclic shifts in order to average the coressponding DC outputs. Nevertheless the difference in the amount of the PAPR reduction for 1 and 8 symbols for averaging is only 0.3 dB at a CCDF of 10^{-4}. In Fig. 3.6, the PAPR reduction for 1, 2, 4, and 8 symbols for averaging are quite close at a CCDF of 10^{-4} with 3 branches and the resolution of $\delta = 8$. The PAPR for 8 symbols for averaging decreases around 0.9 dB as compare to the single branch (Chapter 2) at a CCDF of 10^{-4} with the same number of SCs. Therefore, the PAPR performance with multiple branches is better than the single branch.

3.3.4. Accuracy Rate and BER Performance

The accuracy rate is the ratio of correct estimation in term of the amounts of the

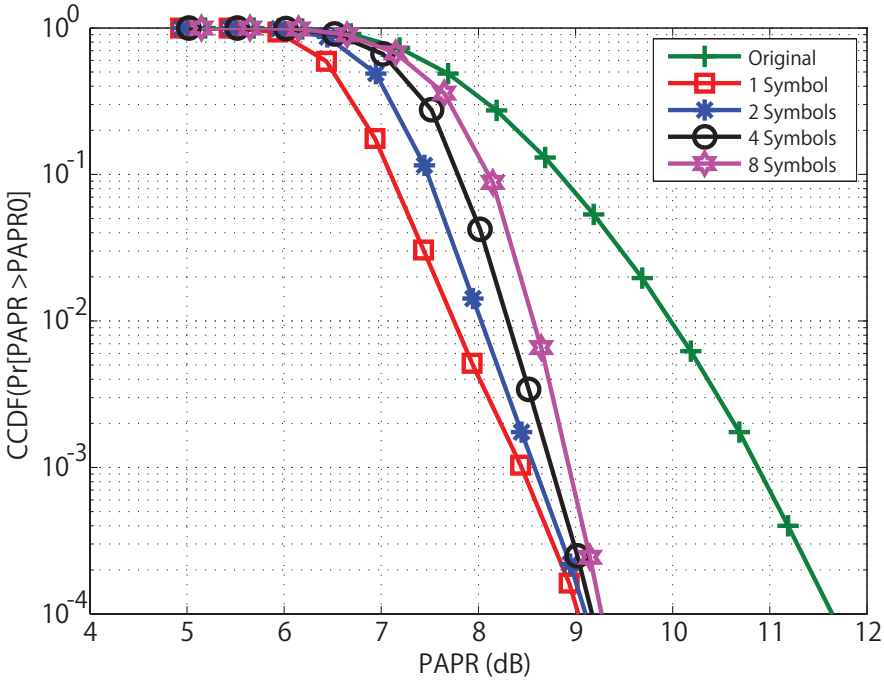

Figure 3.5: PAPR reduction Resolution=4.

cyclic shifts in the receiver side. The accuracy rate of the cyclic shift estimation is shown in Fig. 3.7. Here, the uniform delay profile channel is assumed. In Fig. 3.7, the accuracy rate of the proposed scheme for 1, 2, 4, or 8 symbols for averaging are around 57.04 %, 87.80 %, 98.28 %, and 100%, respectively, at $E_b/N_0 = 5$ dB. The multipath channel effects the accuracy rate of the cyclic shift estimation. It is observed that the accuracy rates of the proposed scheme with 8 symbols for averaging achieves the highest as compared to the others. The accuracy rates of the proposed scheme and the conventional TDC-SLM with 8 symbols for averaging reach 100 % at $E_b/N_0 = 5$ and $E_b/N_0 = 7$ dB, for 8 symbols for averaging, respectively. The accuracy rate performance is 2 dB better as compared to that of the conventional TDC-SLM scheme.

The accuracy rate effects on the BER performance. The BER performance of the proposed scheme and the conventional TDC-SLM scheme with 8 symbols for averaging is presented in Fig. 3.8 on the uniform delay profile channel. The difference between the BERs with perfect estimation and the proposed scheme with 8 symbols for averaging is 0.6 dB and it is 0.2 dB better than that of the conventional TDC-SLM scheme.

The BER and the accuracy rate with the HPA are also evaluated. Figure 3.9 presents the comparison of the accuracy rate between the proposed scheme and the conventional TDC-SLM. The number of the symbols for averaging is set to 8. The accuracy rate of the propose scheme reaches 100 % when E_b/N_0=10 dB, 11 dB, and 13 dB for IBO

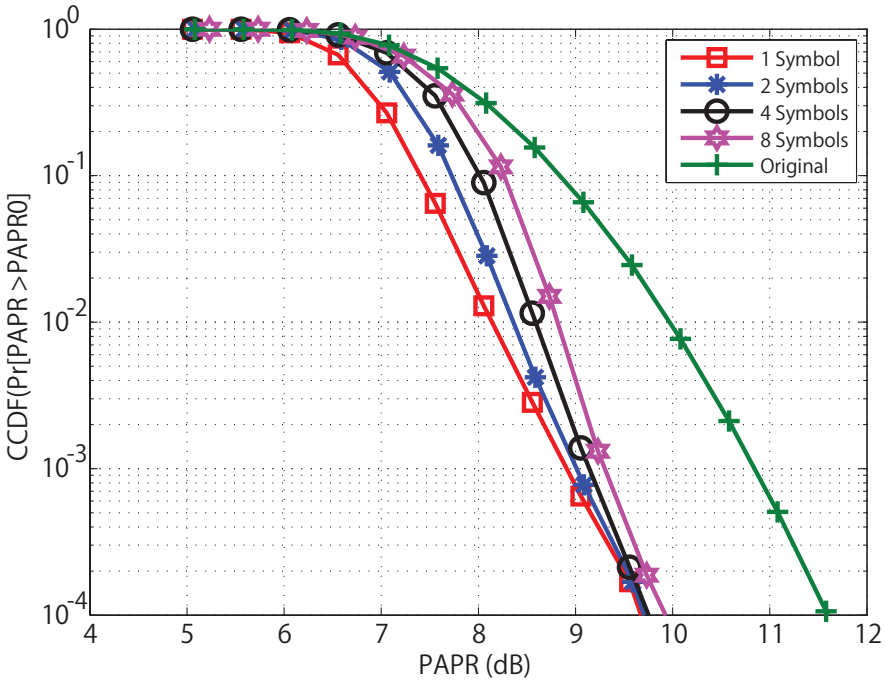

Figure 3.6: PAPR reduction for Resolution=8.

of 4 dB, 2 dB, and 0 dB, respectively. On the other hand, the accuracy rate of the conventional TDC-SLM realizes 100 % at E_b/N_0= 11 dB, 12 dB, and 14 dB for IBO of 4 dB, 2 dB, and 0 dB, respectively. It shows that the accuracy rate of the proposed scheme improves when the DC-MF is placed after FDE-MMSE even though the nonlinierity of the HPA is assumed. The accuracy rate performance is 1 dB better as compared to that of the conventional TDC-SLM scheme. The BERs for the different values of the IBO are also evaluated as depicts in Fig. 3.10. In the conventional TDC-SLM, the required E_b/N_0 values at a BER of 10^{-3} are 13 dB, 13.3 dB, and 13.8 dB, for IBO of 4 dB, 2 dB, 0 dB, respectively. On the other hand, with the proposed scheme, it is 12.8 dB, 13.1 dB, and 13.3 dB for IBO of 4 dB, 2 dB, and 0 dB, respectively. It is observed that the BER improves by increasing the IBO. The BER differences between the conventional TDC-SLM and the proposed scheme are 0.4 dB, 0.3 dB, and 0.4 dB at a BER of 10^{-3} for IBO of 4 dB, 2 dB, and 0 dB, respectively. The proposed scheme is proven to improve the accuracy rate and the BER performance as they approach to the values with perfect estimation.

3.3.5. The Resolution Effect for the Performance System

The resolution is provided to minimize the effect of the multipath fading. When the DC output is shifted due to the multipath fading, it causes the incorrect estimation of

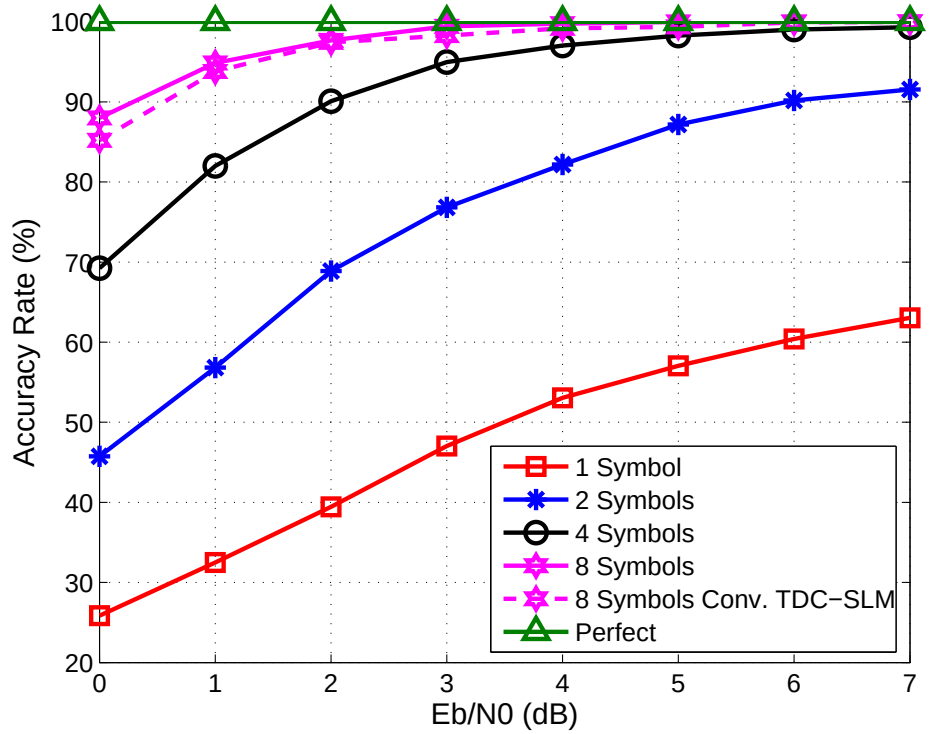

Figure 3.7: Accuracy rate on uniform delay profile channel.

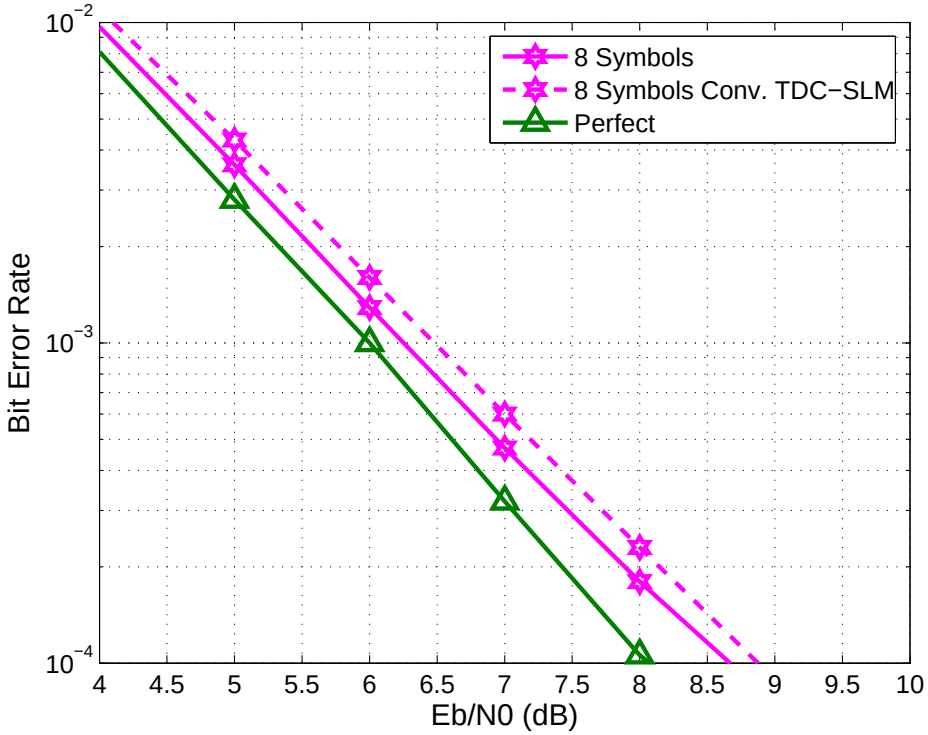

Figure 3.8: BER on uniform delay profile channel.

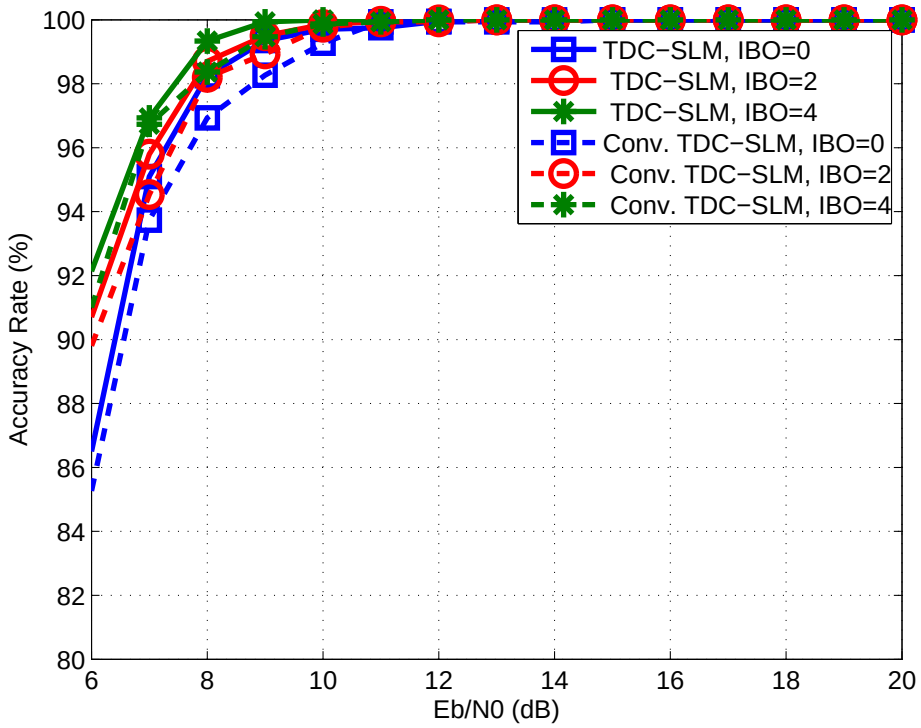

Figure 3.9: Accuracy rate with HPA on uniform delay profile channel.

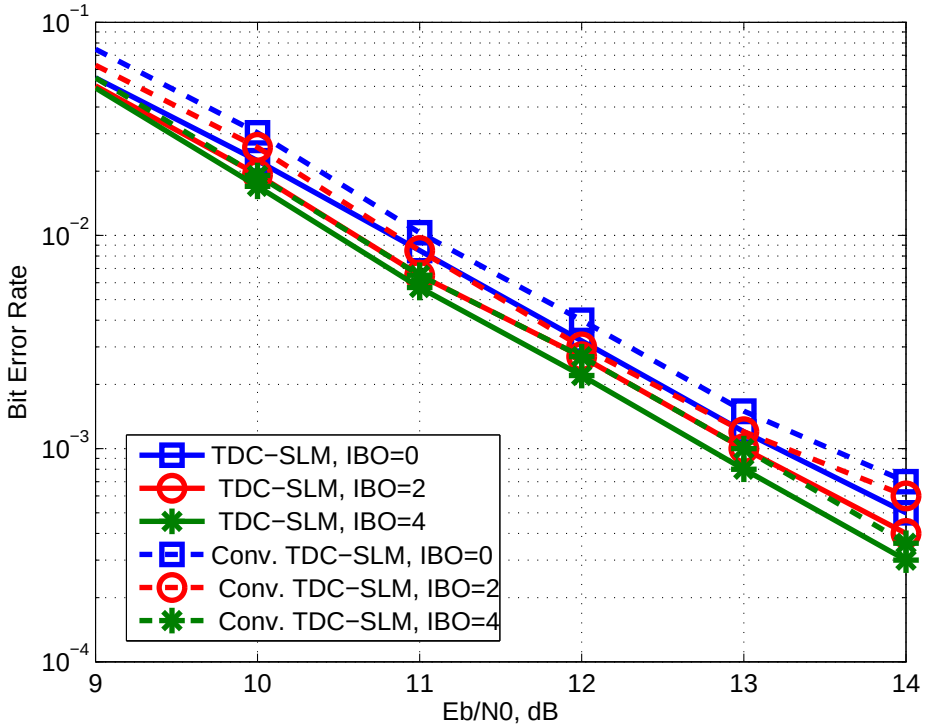

Figure 3.10: BER with HPA on uniform delay profile channel.

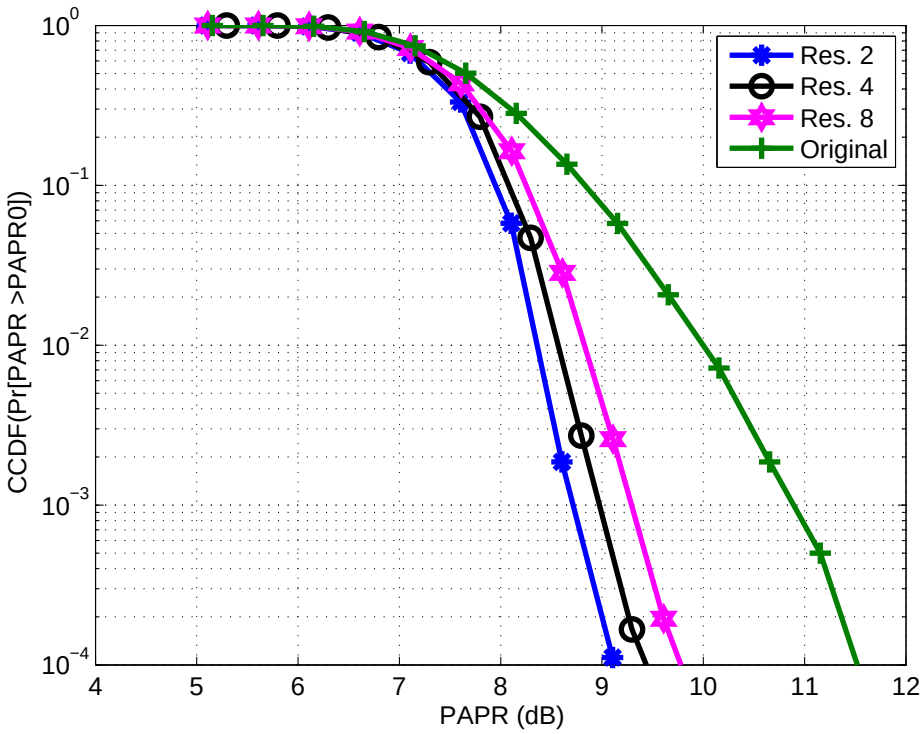

Figure 3.11: PAPR Performance for Different Resolution.

cyclic shift at the receiver side. In this section, the performance of the proposed scheme is evaluated with a different of resolutions (δ). In Fig. 3.11, the PAPR performance at δ=2 is better than δ=4 or δ=8 because the number of SCs with δ=2 is more than δ=4 or δ=8 therefore the probability to achieve lower PAPR is larger. The BER performance and the accuracy rate is evaluated at non-linear HPA Rapp SSPA with IBO=4 and knee factor of 3. The accuracy rate for δ=4 and δ=8 are close to 100 % while the accuracy rate of δ=2 is 95.67 % at E_b/N_0 = 10 dB as shown in Fig. 3.12. When small resolution is applied, the accuracy rate is highly affected by the multipath fading resulting in inaccurate cyclic shift estimation. The BER differences between δ=4 and δ=8 are quite close at a BER of 10^{-3}. On other hand, the BER difference of δ=2 and δ=4 is more than 1 dB at a BER of 10^{-3} as seen in Fig. 3.13.

3.4. Conclusions

In this chapter, the SI detection scheme for the TDC-SLM has been proposed. The DC-MF is implemented after the MMSE detection to remove the effect of the multipath channel. The amount of PAPR reduction with the TDC-SLM is around 2.5 dB as compared with that of the original signal for 8 symbols for averaging when the resolution of the cyclic shift is $\delta = 4$ samples. The accuracy rate of the proposed scheme reaches

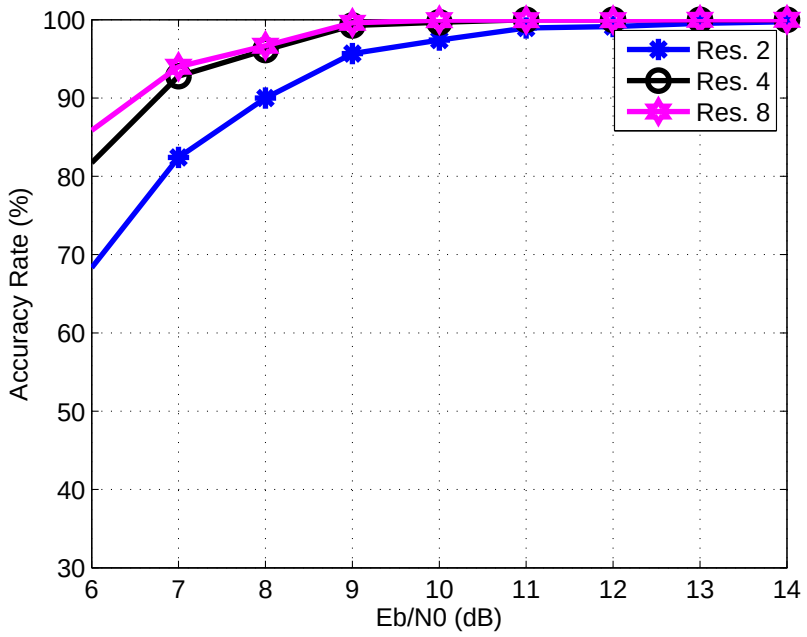

Figure 3.12: Accuracy Rate for Different Resolution.

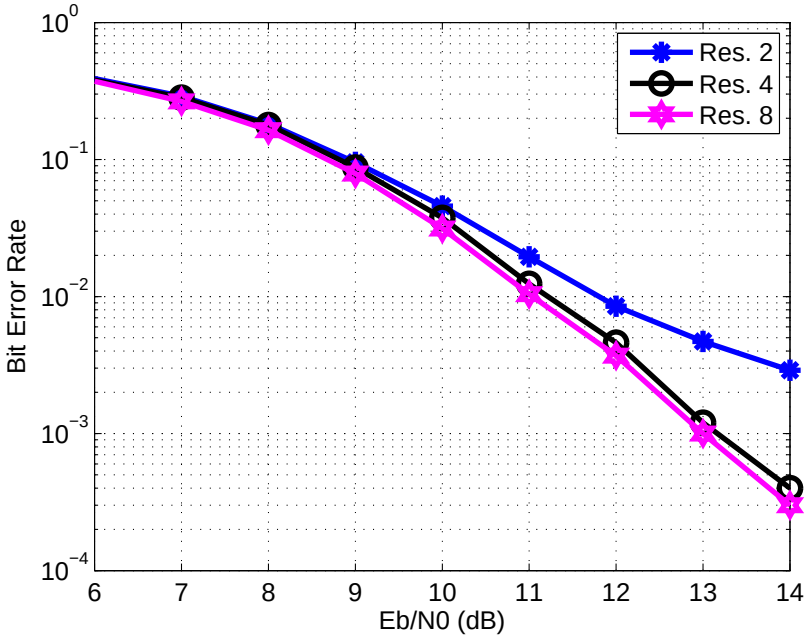

Figure 3.13: BER Performance for Different Resolution.

100 % at E_b/N_0=5 dB and the BER difference with 8 symbols for averaging is around 0.6 dB as compare to that with the perfect estimation of the SI. The BER is 0.2 dB better than that of the conventional TDC-SLM scheme. Under the nonlinierity of the HPA, the proposed scheme still improves the BER performance by around 0.4 dB at a BER of 10^{-3} for IBO of 4 dB, 2 dB, and 0 dB.

Chapter 4

Overall Conclusions

The PAPR of the OFDM transmitted signal determines the power efficiency of the HPA. Therefore, reducing the PAPR of the OFDM signal is essential as power efficient in wireless communication relates to coverage range, power consumption and the size of the terminals. TDC-SLM scheme is one of the distortionless PAPR reductions which generate the SCs by summing the original signal and its cyclic delayed versions. The SC with the lowest PAPR is selected for transmission. However, the TDC-SLM requires SI to recover data in the receiver side. The sending of SI is critical issues in TDC-SLM scheme because the throughput degradation. This dissertation is proposed cyclic shift estimation schemes to omit the SI transmission.

4.1. DC Scheme for Cyclic Shift Estimation

The delayed correlation based estimation scheme is proposed in this dissertation to omit the transmission of the SI. The proposed scheme exploits the correlation between the guard interval sequence and the received signal with delay to estimate the amount of the cyclic shift at the receiver side. The largest peak appears when the last part of the OFDM symbol is multiplied with the conjugate of the GI. The distance of the largest peak to the second peak is indicated the cyclic shift estimation. The impulse response will be shifted with amount of cyclic shift estimation, Δ, and summed together with the original data. Numerical results obtained through computer simulation show that the proposed scheme can estimate the cyclic shift with an accuracy of more than 0.99 at an E_b/N_0 of 8 dB and achieve the PAPR reduction performance that is better than the conventional SLM while the bit error rate degradation is slightly different from that with perfect shift estimation.

4.2. DC-MF Scheme for Cyclic Shift Estimation

In the DC scheme uses the symbol for averaging in order to reduce the effect of the channel for the accuracy rate. When it is applied, the DC scheme has a trade-off between PAPR reduction and the BER. The DC-MF scheme is proposed to recover that limitation. At the transmitter side, the multiple branches is used to generate the SCs. It has restriction in to reduce the number of combination for cyclic shift by using Barker code sequences. The structure of MF has delay line in which all the delay set to $(\delta - 1)$. In the proposed scheme, the DC-MF is placed after the FDE to improve the accuracy of cyclic shift estimation. The accuracy rate of the propose scheme reaches 100 % at E_b/N_0= 5 dB and the BER improves 0.2 dB as compared with the conventional TDC-SLM. The BER performance of the proposed scheme is also better than that of the conventional TDC-SLM even though a nonlinear high power amplifier is assumed.

4.3. Future Work

There are still many challenges for improving the PAPR reduction performance with time domain selective mapping and cyclic shift estimation. First, the coefficient of the matched filter can be set some values other than 1 and -1 to improve the PAPR reduction. Second, the cyclic delay estimation schemes can be implemented at LTE which is required to be modified at the transmitter and receiver sides because in the multiuser LTE each user has a different cyclic delay for reduce PAPR. Third, filter-OFDM which is one of the candidates for 5G therefore it still has PAPR problem and causes interference among subcarriers. TDC-SLM with cyclic shift estimation can be developed to meet the requirement of filtered-OFDM system.

References

[1] Y. Rahmatallah and S. Mohan, "Peak-to-Average Power Ratio Reduction in Ofdm System: A survey and Taxonomy," *IEEE Communication Surveys Tutorials*, vol. 15, no. 4, pp. 1567 – 1592, April 2013.

[2] T. Jiang and Y. Wu, "An Overview: Peak-to-Average Power Ratio Reduction Technique for OFDM Signals," *IEEE Trans. on Broadcast*, vol. 54, no. 2, pp. 257 – 268, June 2008.

[3] S. H. Han and J. H. Lee, "An Overview of Peak to Average Power Ratio Reduction Technique Multicarrier Transmission," *IEEE Wireless communication*, vol. 12, no. 2, pp. 56 – 65, July 2005.

[4] M. Rahnema, "Overview of the GSM System and Protocol Architecture," *IEEE Commun. Mag.*, vol. 31, no. 4, pp. 92 – 100, April 1993.

[5] P. Chaudhury, W. Mohr, and S. Onoe, "The 3GPP Proposal for IMT-2000," *IEEE Commun. Mag*, vol. 37, no. 12, pp. 72 – 81, Dec. 1999.

[6] E. Dahlman, B. Gudmundson, M. Nilsson, and A. Skold, "UMTS/IMT-2000 Based on Wideband CDMA," *IEEE Commun. Mag.*, vol. 36, no. 9, pp. 70 – 80, Sept. 1998.

[7] B. Crow, I. Widjaja, L. Kim, and P. Sakai, "IEEE 802.11 Wireless Local Area Networks," *IEEE Commun. Mag.*, vol. 35, no. 9, pp. 116–126, Sept. 1997.

[8] E. Perahia, "IEEE 802.11n Development: History, Process, and Technology," *IEEE Commun. Mag*, vol. 46, no. 7, pp. 48 – 55, July 2008.

[9] L. Venn, M. Fakharzadeh, and S. Choi, "Wifi on Steroids: 802.11ac and 802.11ad," *IEEE Wireless Communications*, vol. 20, no. 6, pp. 30 – 35, Dec. 2013.

[10] E. Perahia, C. Cordeiro, M. Park, and L.L. Yang, "IEEE 802.11ad: Defining the Next Generation MultipGbps Wi-fi," *Proc. 7th IEEE Consumer Communications and Networking Conference*, pp. 1 – 5, Jan. 2010.

[11] T. S. Rappaport, *Wireless Communications, Principles and Practice.* New Jersey: Prentice Hall, 1996.

[12] M. L. Doelz, E. T. Heald, and D. L. Martin, "Binary Data Transmission Techniques for Linear Systems," *Proc IRE*, vol. 45, pp. 656–661, May 1957.

[13] J. Bingham, "Multicarrier Modulation for Data Transmission: an Idea Whose Time Has Come," *IEEE Commun. Mag.*, vol. 28, no. 5, pp. 5 – 14, May 1990.

[14] L. J. Cimini Jr, Ye, L., "Orthogonal Frequency Division Multiplexing for Wireless Channels," *IEEE Global Telecommunications Conference GLOBECOM*, 1998.

[15] R. Prasad and R. van Nee, *OFDM for Wireless Multimedia Communications.* Boston, Artech House, 2000.

[16] S. C. Thompson, J. G. Proakis, and J. R Zeidler, "The Effectiveness of Signal Clipping for PAPR and Total Degradation Reduction in OFDM Systems," *IEEE Commun. Society*, 2008.

[17] C. Ramp, "Effects of HPA-Nonlinearity on a 4-DPSK/OFDM-Signal for a Digital Sound Broadcasting Signal," *Proc. 2nd Europ. Conf. Sattelite Commun.*, pp. 179 – 184, Oct. 1991.

[18] S. H. Han and J. H. Lee, "Peak-to-average Power Ratio Reduction of an OFDM Signal by Signal Set Expansion," *in Proc. IEEE Int. Conf. Commun.*, vol. 2, pp. 867 – 971, 2004.

[19] N. Chaudhary and L.Cao, "IEEE Comparison of Compand-Filter Schemes for Reducing PAPR in OFDM," *Wireless Communications and Networking Conference*, vol. 4, pp. 2070 – 2075, 2006.

[20] Y. S. Cho, J. Kim, W. Y. Yang, and C. G. Kang, *MIMO-OFDM Wireless Communication with Matlab.* John Wiley and Sons (Asia), 2010.

[21] L. Wang, C. Tellambura, "Clipping Noise Guide Sign-Selection for PAR Reduction in OFDM Systems," *IEEE Trans. on Signal Processing*, vol. 56, pp. 5644–5653, 2008.

[22] S. Kimura, T. Nakamura, M. Saito and M. Okada, "PAR Reduction for OFDM Signals Based on Deep Clipping," *3rd International Symposium on Communications,Control and Signal Processing*, pp. 911 –916, March 2008.

[23] M. Wang, D.E. Quevedo, G.C. Goodwin, B.S. Krongold, "OFDMA Uplink PAR Reduction via Tone Reservation," *IEEE Globecom*, pp. 3802 – 3806, 2007.

[24] S. H. Muller, J.B. Huber, "OFDM with Reduced Peak-to-average Power Ratio by Multiple Signal Representation," *IET Electronic Letters*, vol. 33, pp. 368 – 369, 1997.

[25] T. Horiuchi, T. Ohtsuki, and I. Sasase, "Performance Evaluation of OFDM with a Nonlinear Distortion Compensation Technique Using Partial Transmit Sequence and Predistortion," *Electronics and Communications*, vol. 87, no. 6, pp. 34–42, 2004.

[26] S. G. Kang, J. G. Kim, and E. Kyeong, "A Novel Subblock Scheme for Partial Transmit Sequence OFDM," *IEEE Trans. on Broadcasting*, vol. 45, no. 3, pp. 313 – 338, March 1999.

[27] N. Ohkubo, and T. Ohtsuki, "Design Criteria for Phase Sequences in Selected Mapping," *IEICE Trans. Commun*, vol. E86-B, no. 9, pp. 2628–2636, Sept. 2003.

[28] ——, "A Peak to Average Power Ratio Reduction of Multicarrier CDMA Using Selected Mapping," *VTC-Fall*, Sept. 2002.

[29] C. L. Wang and Y. Ouyang, "Low-Complexity Selected Mapping Schemes for Peak-to-Average Power Ratio Reduction in OFDM Systems," *IEEE Trans. on Signal Processing*, vol. 53, no. 12, pp. 4652 – 4660, Dec. 2005.

[30] L. Yang, K. K. Soo, Y. M. Siu, and S. Q. Li, "A Low-complexcity Selected Mapping Scheme by Use of Time Domain Sequence Superposition Technique for PAPR Reduction in OFDM System," *IEEE Trans. Broadcast*, vol. 54, no. 4, pp. 821 – 824, Dec. 2008.

[31] A. Boonkajay, T. Obara, T. Yamamoto, and F. Adachi, "Selective Mapping for Broadband Single-Carrier Transmission Using Joint Tx/Rx MMSE-FDE," *24th PIMRC*, Sept. 2013.

[32] J. S. Wang,J. C. Park, I.Song, and Y. H. Kim, "Combining of Cyclically Delayed Signals: A Low-Complexity Scheme for PAPR Reduction in OFDM Systems," *IEEE Trans. on Broadcasting*, vol. 56, no. 4, Dec. 2010.

[33] J. Ji and G. Ren, "A New Modified SLM Scheme for Wireless OFDM Systems without Side Information," *IEEE Trans. on Signal Processing*, vol. 20, no. 11, Nov 2013.

[34] S. S. Eom, H. Nan, and Y. C. Ko, "Low-Complexity PAPR Reduction Scheme without Side Information for OFDM Systems," *IEEE Trans. on Signal Processing*, vol. 60, no. 7, pp. 3657 – 3669, July 2012.

[35] S. Y. Le Goff, S. S. Al-Samahi, B. K. Khoo, C. C. Tsimenidis, and B. S. Sharif, "Selected Mapping without Side Information for PAPR Reduction in OFDM," *IEEE Trans. on Wireless Commun.*, vol. 8, no. 7, pp. 3320 – 3325, July 2009.

[36] E. F. Badran and A. M. El-Helw, "A Novel Semi-Blind Selected Mapping Technique for PAPR Reduction in OFDM," *IEEE Signal Processing Letters*, vol. 18, no. 9, pp. 493 – 496, Sep. 2011.

[37] J. Park, E. Hong, and D. S. Har, "Low Complexity Data Decoding for SLM Based OFDM Systems without Side Information," *IEEE on Commun. Letters*, vol. 15, no. 6, pp. 611 – 613, June 2011.

[38] K. Bae, C. Shin, and E. J. Powers, "Performance Analysis of OFDM Systems with Selected Mapping in the Presence of Nonlinierity," *IEEE Trans. on Wireless Communication*, vol. 12, pp. 2314 – 2322, May 2013.

[39] J. S. Wang, S. H. Hwang, C. J. Kim, and Y. H. Kim, "Time-Domain Signal Combining with Cyclic Delay and Phase Shift for PAPR Reduction in OFDM System," *IEEE International Conference on Consumer Electronics*, Jan. 2011.

[40] S. J. Heo, H. S. Noh, J. S. No, and D. J. Shin, "A Modified SLM Scheme with Low Complexity for PAPR Reduction of OFDM Systems," *IEEE Trans. on Broadcasting*, vol. 53, no. 4, pp. 804 – 808, Dec. 2007.

[41] H. B. Jeon, J. S. No, and D. J. Shin, "A Low-Complexity SLM Scheme using Additive Mapping Sequences for PAPR Reduction of OFDM Signals," *IEEE Trans. on Broadcasting*, vol. 57, no. 4, pp. 866 – 875, Dec. 2011.

[42] E. Hong, H. Kim, K. Yang, and D. S. Har, "Pilot-Aided Side Information Detection in SLM-Based OFDM Systems," *IEEE Trans. on Wireless Commun.*, vol. 12, no. 7, pp. 3140–3147, July 2013.

[43] A. Boonkajay, F. adachi, "Low-PAPR Joint Transmit/Received SC-FDE transmission Using Time Domain Selected Mapping," *Asia-Pacific Conference onCommunication*, Oct. 2014.

[44] P. D. Pamungkasari and Y. Sanada, "Time Domain Cyclic-Selective Mapping for PAPR Reduction using Delayed Correlation with Matched Filter in OFDM System,," *IEEE Vehicular Technology Conference*, May 2015.

[45] ——, "PAPR Reduction Using Cyclic-Selective Mapping with Delayed Correlation in Time Domain," *International Conference on Telecommunications*, pp. 373 – 377, April 2015.

List of Achievements

Journal Publications

1. P.D. Pamungkasari and Y. Sanada, "Shift Estimation with Delayed Correlation Cyclic-Selective Mapping (Cyclic-SLM) PAPR Reduction in OFDM System," Wireless Personal Communication, July 2016.

2. P.D. Pamungkasari and Y. Sanada, "Estimation of Cyclic Shift with Delayed Correlation and Matched Filtering in Time Domain Cyclic-SLM for PAPR Reduction," International Scholarly Research Notices, vol. 2016, Sept. 2016.

Conference Publications

1. P. D. Pamungkasari and Y. Sanada, "PAPR Reduction Using Cyclic-Selective Mapping with Delayed Correlation in Time Domain," 81st IEEE Vehicular Technology Conference, May 2015.

2. P. D. Pamungkasari and Y. Sanada, "Time Domain Cyclic-Selective Mapping for PAPR Reduction using Delayed Correlation with Matched Filter in OFDM System," The 22nd International Conference on Telecommunications, pp. 373 - 377, April 2015.

Technical Reports

1. P. D. Pamungkasari, Y. Sanada, "Time Domain Delayed Correlation based Cyclic Delay Estimation for Low Complexity Cyclic-Selective Mapping in OFDM System," IEICE Technical Report, vol. 114, no 164, RCS2014-93, July. 2014.

2. P. D. Pamungkasari, Y. Sanada, "Cyclic Shift Estimation with Delayed Correlation and Matched Filtering in Cyclic-SLM PAPR Reduction," IEICE Technical Report, vol. 114, no 402, CS2014-90, Jan. 2015.

Presentations at Domestic Meeting

1. P. D. Pamungkasari, Y. Sanada, "Improvement on PAPR for Filtered OFDM,"Communication Quality Workshop, August 2016.

Appendix
Selection Criteria for Symbols Averaging

Selection Criteria for Symbols Averaging

This subsection explains the relationship between selection criteria for more than 1 symbol for averaging. The original signal is summed with its cyclically shifted signal as follows

$$\tilde{x}_{v,m}[n] = x_v[n] + x_v[n, \Delta_{d,m}] \tag{A-1}$$

where Δ is the amount of cyclic shift. M is the number of the SCs, $m \in \{1, ..., M\}$, V is the number symbol for averaging, $v \in \{1, ..., V\}$, D is the numberof branches, $d \in \{1, ..., D\}$, and Q_d is used as the phase sequence which follows of the Barker sequence.

$$\begin{aligned} \tilde{x}_{v,m}[n] \quad = \quad & \begin{bmatrix} \mathbf{x}_1[n] + Q_1 x_1[n, \Delta_{1,1}] + & \dots & + Q_D x_1[n, \Delta_{D,1}] \\ \mathbf{x}_1[n] + Q_1 x_1[n, \Delta_{1,2}] + & \dots & + Q_D x_1[n, \Delta_{D,2}] \\ \vdots & \vdots & \vdots \\ \mathbf{x}_1[n] + Q_1 x_1[n, \Delta_{1,M}] + & \dots & + Q_D x_1[n, \Delta_{D,M}] \end{bmatrix} \\ , ..., \quad & \begin{bmatrix} \mathbf{x}_V[n] + Q_1 x_V[n, \Delta_{1,1}] + & \dots & + Q_D x_V[n, \Delta_{D,1}] \\ \mathbf{x}_V[n] + Q_1 x_V[n, \Delta_{1,2}] + & \dots & + Q_D x_V[n, \Delta_{D,2}] \\ \vdots & \vdots & \vdots \\ \mathbf{x}_V[n] + Q_1 x_V[n, \Delta_{1,M}] + & \dots & + Q_D x_V[n, \Delta_{D,M}] \end{bmatrix} \end{aligned} \tag{A-2}$$

M SCs for V symbols can be written as follows

$$\tilde{x}_{v,m}[n] \quad = \quad \begin{bmatrix} \mathbf{x}_{1,1}[n], \mathbf{x}_{2,1}[n], & \dots & \mathbf{x}_{V,1}[n] & \\ \mathbf{x}_{1,2}[n], \mathbf{x}_{2,2}[n], & \dots & \mathbf{x}_{V,2}[n] & \\ \vdots & \vdots & \vdots & \vdots \\ \mathbf{x}_{1,M}[n], \mathbf{x}_{2,M}[n], & \dots & \mathbf{x}_{V,M}[n] & \end{bmatrix} \tag{A-3}$$

The calculation of the average and normalized power for M SCs as follows

$$P_m[n] = \frac{|\tilde{x}_{v,m}[n]|^2}{V * N}$$
$$\tilde{x}_{norm}[n] = \frac{1}{\sqrt{P_m[n]}}\tilde{x}_{v,m}[n] \tag{A-4}$$

The PAPR of M SCs per V symbols are given by

$$\mathrm{PAPR}_m = 10\log\frac{|\tilde{x}_{norm}[n]|^2}{E\,|\tilde{x}_{norm}[n]|^2} \tag{A-5}$$

To select minimum index m for set of PAPR_m

$$m_{\min} = \left\{ m|_{\min\limits_{1\leqslant m\leqslant M}} \mathrm{PAPR}_m \right\} \tag{A-6}$$

The lowest PAPR for per V symbols is calculated as follows

$$\mathrm{PAPR}_v = 10\log\frac{|\tilde{x}_{v,m_{\min}}[n]|^2}{E\,|\tilde{x}_{v,m_{\min}}[n]|^2} \tag{A-7}$$

Acknowledgements

I would like to express my deepest gratitude to my supervisor Prof. Yukitoshi Sanada for supporting me during these past 4 years. I am grateful for the tremendous amount of time he devoted to me and this research. He is one of the smartest people and give a passion in this research. His invaluable advice, constant encouragement, and constructive criticism during the entire period of my PhD study. He guided me to learn and enjoy the world of research. Without his support, I could not yield any achievement and complete my dissertation. I would also like to express my gratitude for the referees who examined this dissertation, Prof. Sasase, Prof. Ikehara, and Prof. Ohtsuki. Their critical reviews and constructive suggestions added an extra layer polish to this dissertation.

I will forever be thankful to my collaboration research advisor Prof. Mohamad Ghavami. He has been helpful in providing advice many times during my graduate school career and in this research.

I am also very grateful to my colleagues in Sanada Laboratory that always give support to surviving and staying in graduate school and living in Japan. I was lucky to be part of this warm and welcome group in Sanada Laboratory.

Furthermore, I would like to appreciate and gratitude the financial support from Ministry of Research, Technology and Higher Education Republic of Indonesia during this study process.

Finally, I would like to express my deep gratitude and love to my family that always give a support, love and care during my PhD study.